TN-333

NUREG/CR-2106
CREARE TN-333


# 1/5-SCALE COUNTERCURRENT FLOW DATA PRESENTATION AND DISCUSSION

TOPICAL REPORT

C. J. Crowley
P. H. Rothe
R. G. Sam

Creare Inc.
Hanover, New Hampshire



Prepared for
U. S. Nuclear Regulatory Commission

Available from

GPO Sales Program
Division of Technical Information and Document Control
U. S. Nuclear Regulatory Commission
Washington, D. C. 20555

Printed copy price: $3.25

and

National Technical Information Service
Springfield, Virginia 22161

Creare TN-333
NUREG/CR-2106
R2

# 1/5-SCALE COUNTERCURRENT FLOW DATA PRESENTATION AND DISCUSSION

Topical Report

Creare Contributors: C. J. Crowley
P. H. Rothe
R. G. Sam

NRC Contributors: W. D. Beckner
J. N. Reyes
S. E. Trenery

Manuscript Completed: April 1981
Date Published: November 1981

Creare, Inc.
Hanover, New Hampshire

Prepared for
Division of Accident Evaluation
Office of Nuclear Regulatory Research
U.S. Nuclear Regulatory Commission
Washington, D.C. 20555

NRC FIN No. A4070

Availability of Reference Materials Cited in NRC Publications

Most documents cited in NRC publications will be available from one of the following sources:

1. The NRC Public Document Room, 1717 H Street., N.W.
   Washington, DC 20555
2. The NRC/GPO Sales Program, U.S. Nuclear Regulatory Commission,
   Washington, DC 20555
3. The National Technical Information Service, Springfield, VA 22161

Although the listing that follows represents the majority of documents cited in NRC publications, it is not intended to be exhaustive.

Referenced documents available for inspection and copying for a fee from the NRC Public Document Room include NRC correspondence and internal NRC memoranda; NRC Office of Inspection and Enforcement bulletins, circulars, information notices, inspection and investigation notices; Licensee Event Reports; vendor reports and correspondence; Commission papers; and applicant and licensee documents and correspondence.

The following documents in the NUREG series are available for purchase from the NRC/GPO Sales Program: formal NRC staff and contractor reports, NRC-sponsored conference proceedings, and NRC booklets and brochures. Also available are Regulatory Guides, NRC regulations in the *Code of Federal Regulations*, and *Nuclear Regulatory Commission Issuances*.

Documents available from the National Technical Information Service include NUREG series reports and technical reports prepared by other federal agencies and reports prepared by the Atomic Energy Commission, forerunner agency to the Nuclear Regulatory Commission.

Documents available from public and special technical libraries include all open literature items, such as books, journal and periodical articles, transactions, and codes and standards. *Federal Register* notices, federal and state legislation, and congressional reports can usually be obtained from these libraries.

Documents such as theses, dissertations, foreign reports and translations, and non-NRC conference proceedings are available for purchase from the organization sponsoring the publication cited.

Single copies of NRC draft reports are available free upon written request to the Division of Technical Information and Document Control, U.S. Nuclear Regulatory Commission, Washington, DC 20555.

## ABSTRACT

Separate effects data for countercurrent flow behavior in a 1/5-scale PWR geometry are presented. The data represent the largest scale data of this type obtained up to the present time. A statistical analysis of these data has been performed and is also included here. The results of the statistical analysis are compared with analyses of data from smaller scale vessels. The trends in the data are consistent with trends indicated by the smaller scale data.

TABLE OF CONTENTS


| | | Page |
|---|---|---|
| | ABSTRACT | iii |
| | LIST OF FIGURES | vii |
| 1 | INTRODUCTION | 1 |
| 2 | FACILITY AND TEST PROCEDURES | 2 |
| 3 | SATURATED ECC DATA | 3 |
| 4 | SUBCOOLED ECC DATA | 6 |
| 5 | CREARE DATA COMPARISONS AND DISCUSSION | 10 |
| | REFERENCES | 15 |
| | APPENDIX A - DATA UNCERTAINTY ANALYSIS | A-1 |
| | APPENDIX B - 1/5-SCALE CCF DATA TABULATION | B-1 |
| | APPENDIX C - STATISTICAL ANALYSIS OF 1/5-SCALE DATA | C-1 |
| | APPENDIX D - CREARE 1/5-SCALE NON-LINEAR LEAST SQUARES STATISTICS | D-1 |

LIST OF FIGURES


| Figure | Title | Page |
|---|---|---|
| 1 | 1/5-SCALE CCF DATA WITH $T_{ECC}$≈212°F AND $J^*_{fin}$≈0.12 PLOTTED ON J* COORDINATES | 4 |
| 2 | COMPARISON OF 1/5-SCALE CCF DATA WITH $T_{ECC}$≈212°F AND $T_{ECC}$≈145°F ($J^*_{fin}$≈0.12) PLOTTED ON J* COORDINATES | 7 |
| 3 | COMPARISON OF 1/5-SCALE CCF DATA WITH $T_{ECC}$≈212°F AND $T_{ECC}$≈205°F ($J^*_{fin}$≈0.12) PLOTTED ON J* COORDINATES | 8 |
| 4a | UNUSUAL PLENUM FILLING DATA WITH $J^*_{gc}$≈0.05, $T_{ECC}$≈205°F AND $J^*_{fin}$≈0.12 | 9 |
| 4b | TYPICAL PLENUM FILLING DATA WITH $J^*_{gc}$≈0.05, $T_{ECC}$≈212°F AND $J^*_{fin}$≈0.12 | 9 |
| 5 | COMPARISON OF CCF DATA AT 1/5, 1/15, AND 1/30 SCALES WITH $T_{ECC}$≈212°F AND $J^*_{fin}$≈0.12 PLOTTED ON J* COORDINATES | 11 |
| 6 | COMPARISON OF CCF DATA AT 1/5 AND 1/15 SCALES WITH $T_{ECC}$≈212°F AND $J^*_{fin}$≈0.06 PLOTTED ON J* COORDINATES | 12 |
| 7 | COMPARISON OF CCF DATA AT 1/5 AND 1/15 SCALES WITH $T_{ECC}$≈145°F AND $J^*_{fin}$≈0.12 PLOTTED ON J* COORDINATES | 13 |
| 8 | COMPARISON OF CCF DATA AT 1/5, 1/15 AND 1/30 SCALES WITH $T_{ECC}$≈212°F AND $J^*_{fin}$≈0.12 PLOTTED ON K* COORDINATES | 14 |
| A-1 | LOWER PLENUM FLUID TEMPERATURE FOR A TYPICAL CCF TEST | A-3 |
| A-2 | TEMERATURE OF STEAM ENTERING VESSEL FOR A TYPICAL CCF TEST | A-3 |
| C-1 | GAS FLOW FOR COMPLETE BYPASS (WITHOUT CONDENSATION) AS A FUNCTION OF SCALE SIZE USING EQUATION C-1 | C-4 |
| C-2 | GAS FLOW FOR COMPLETE BYPASS (WITHOUT CONDENSATION) AS A FUNCTION OF SCALE SIZE USING EQUATION C-2 | C-4 |
| C-3 | CONDENSATION EFFICIENCY AS A FUNCTION OF SCALE SIZE USING EQUATION C-1 | C-5 |
| C-4 | CONDENSATION EFFICIENCY AS A FUNCTION OF SCALE SIZE USING EQUATION C-2 | C-5 |
| C-5 | SLOPE OF PENETRATION CURVE (WITHOUT CONDENSATION) AS A FUNCTION OF SCALE SIZE USING EQUATION C-1 | C-6 |
| C-6 | SLOPE OF PENETRATION CURVE (WITHOUT CONDENSATION) AS A FUNCTION OF SCALE SIZE USING EQUATION C-2 | C-6 |
| C-7 | CALCULATED SLOPE OF PENETRATION CURVE AS A FUNCTION OF ECC PENETRATION FLOW AT VARIOUS SCALES USING BCL MODEL [9] | C-7 |
| C-8 | EFFECT OF CONDENSATION ON SLOPE OF PENETRATION CURVE AS A FUNCTION OF SCALE SIZE USING EQUATION C-1 | C-8 |

LIST OF FIGURES


| Figure | Title | Page |
|---|---|---|
| C-9 | EFFECT OF CONDENSATION ON SLOPE OF PENETRATION CURVE AS A FUNCTION OF SCALE SIZE USING EQUATION C-2 . . . . . | C-8 |
| C-10 | COMPARISON OF BCL 1/15 (60°-120° COLD LEG) CORRELATION WITH BCL 1/15 (90°-90° COLD LEG) DATA . . . . . | C-9 |
| C-11 | COMPARISON OF CREARE 1/15 (90°-90° COLD LEG) CORRELATION WITH BCL 1/15 (90°-90° COLD LEG) DATA . . . . . | C-11 |
| D-1 | COMPARISON OF CREARE 1/5 SCALE DATA WITH THE TRADITIONAL FORMULATION OF EQUATION C-1 . . . . . | D-3 |
| D-2 | COMPARISON OF CREARE 1/5 SCALE DATA WITH THE MODIFIED FORMULATION OF EQUATION C-2 . . . . . | D-5 |

# 1 INTRODUCTION

Countercurrent flow data from a 1/5-scale model of a PWR vessel are presented and discussed in this memorandum. These data represent the largest scale separate effects tests of countercurrent flow conducted to date. Data with virtually saturated ECC are presented at two injection flow rates ($J^*_{fin}$=0.12 and 0.06). Data at subcoolings of about 70 and 10°F are also presented for one flow rate ($J^*_{fin}$=0.12). These 1/5-scale data are compared graphically with Creare data at 1/15 and 1/30 scales and with BCL 2/15-scale CCF data. Data listings are included in Appendix B.

A statistical analysis of the 1/5-scale experimental data was performed by Beckner et al. using techniques previously developed by NRC [8]. The results of this analysis are presented in Appendix C and compared with results at smaller vessel scales. The 1/5-scale data are consistent with the trends of the data observed at smaller scale.

## 2 FACILITY AND TEST PROCEDURES

The 1/5-scale experimental facility has been described in detail in Reference 1 as it was used for flashing transients. The only modification for these CCF tests was the replacement of the break piping by a straight section of 17 in. ID piping. The oversized break leg was used in order to minimize vessel pressure (and hence ECC subcooling). ECC was injected through three cold legs located at 90° intervals around the vessel circumference from the broken cold leg. Important dimensions of the vessel are summarized in Table 1.

TABLE 1
1/5 SCALE VESSEL DIMENSIONS

| Parameter | Value |
|---|---|
| Gap Size | 1.5 ± 0.050 |
| Average Annulus Circumference | 105.6 ± 0.2 in. |
| Vessel ID | 35.125 ± 0.050 in. |
| Downcomer Length | 54 in. |
| Intact Cold Leg ID | 5.8 in. |
| Broken Cold Leg ID | 17.2 in. |

The tests were conducted by initially heating the ECC in the supply tank to the desired temperature (via a recirculation loop described in Reference 1). In practice, for tests with saturated ECC, $T_{ECC}$ was 212°F for steam flows near the complete delivery point while the ECC was heated a few degrees hotter (up to 215°F) for tests approaching the complete bypass point. The reason for this was to minimize the subcooling to the extent achievable as the vessel pressure increased due to the increased pressure drop across the break at the higher steam flows.

After the steam flow is set, ECC is injected at a preset flow rate. The plenum is allowed to fill, or the test run long enough to establish a filling rate. Steam and water effluent bypassed from the test vessel during this filling are returned to a gas space in the supply tank. The water falls to the supply pool and the steam is exhausted at a top vent.

## 3 SATURATED ECC DATA

The presentation of the data is divided into two groups, one dealing with nearly saturated ECC (this section) and one with subcooled ECC (Section 4). The purpose of the saturated ECC tests is to establish the baseline flooding behavior with little or no effect of condensation. To that end, the ECC subcooling has been minimized as discussed in Section 1. Two nominal ECC flow rates of 1000 and 500 gpm have been tested corresponding to dimensionless flows of $J^*_{fin}$=0.12 and 0.06 respectively.

The results are plotted on the usual dimensionless first power and square-root J* coordinates in Figure 1. Two test procedures called "heated" and "neutral" are identified and are described in detail below. For the moment, ignore the distinction. The data at both flow rates overlay within the range of typical experimental scatter. This is expected based on previous steam/water testing at 1/15-scale [2] and air/water testing at 2/15 scale [3]. The subcoolings for selected data points are based on the saturation temperature at the measured vessel pressure minus the measured ECC temperature and are indicated by numbers shown alongside data points. The maximum subcooling is 11°F for $J^*_{fin}$=0.12 and 5°F for $J^*_{fin}$=0.06.

### Hypothetical Effect of Wall Temperature

During these experiments we observed that the steam temperature at the vessel inlet was as high as 300°F, i.e., superheated approximately 90°F at atmospheric pressure. This situation was without precedent since smaller facilities at Creare and BCL had always had long runs of piping such that condensation reduced the steam to saturation temperature prior to metering and supply to the test vessel. The superheated steam temperatures have a secondary effect on steam properties that can be accounted for analytically (see the discussion of data reduction procedures in Appendix A). We also hypothesized that there might be a significant "hot wall" effect of steam superheat if the walls were in turn superheated during the pretest procedures. To show that this wall heating effect was negligible, we performed diagnostic measurements and did special tests with alternate test procedures.

Our normal procedure, which is referred to in this report as "heated" wall, is to establish steam flow at the rate to be tested and flow steam through the vessel for long periods (several minutes). This process serves to purge air from the vessel and bring the entire system to an initial "equilibrium" state in terms of temperature and flow distributions. The only shock to the flow is the abrupt injection of ECC. Vessel wall temperatures were measured by surface thermocouples to be within 5°F of saturation temperature once this initial equilibrium state was established. Thus, even though the steam was approximately 90°F superheated, the outer vessel walls were at saturation temperature. We hypothesized, and confirmed by some quick calculations, that the heat flux through the uninsulated vessel walls was ample to maintain a thin liquid flim on the wall and establish saturation temperature there. Accepting this mechanism, we would expect the core barrel wall to be at steam temperature, at most 300°F and as low as 212°F at the lower steam flow rates corresponding to the complete delivery point on the penetration curve.

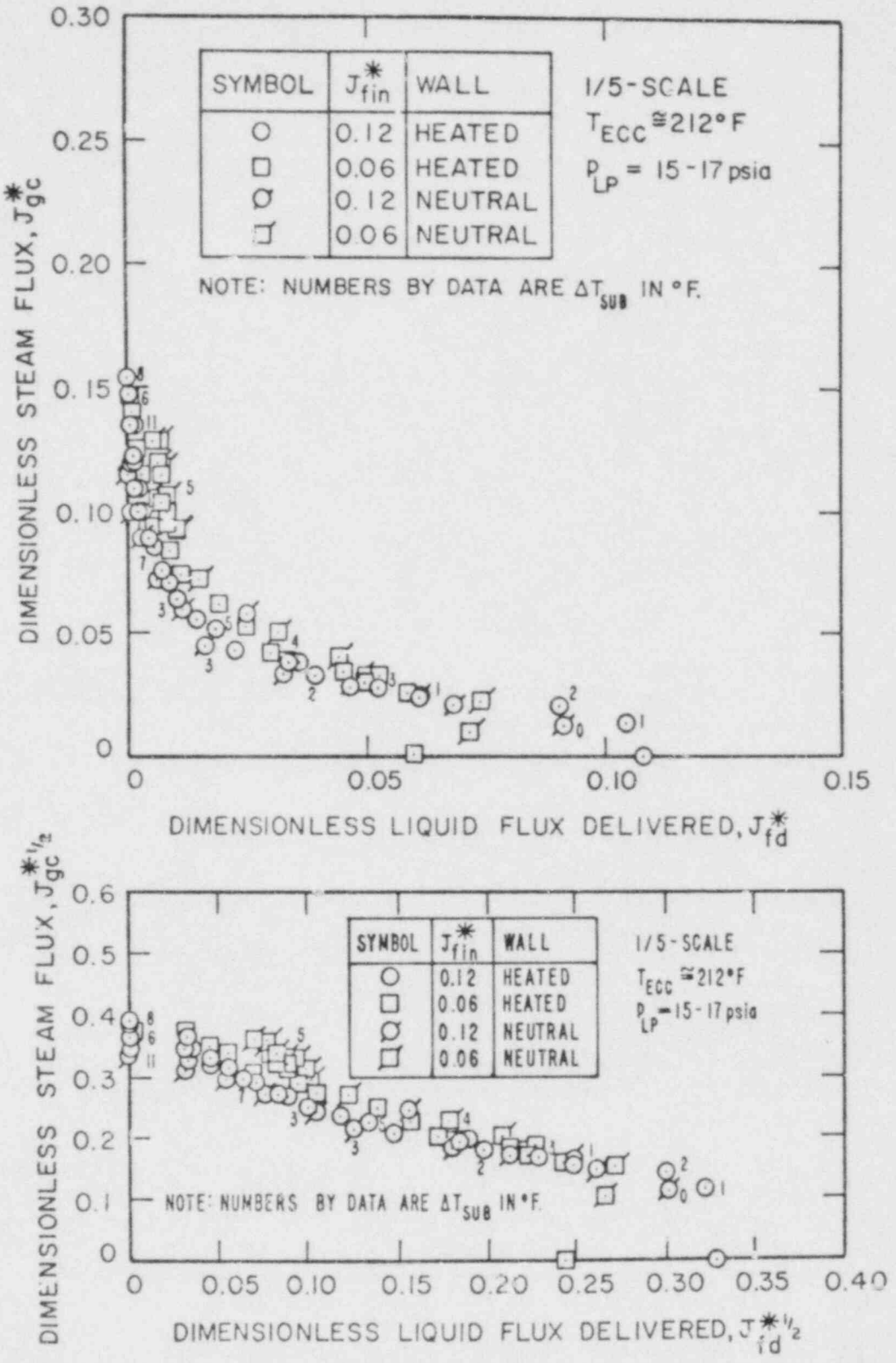


Figure 1. 1/5-SCALE CCF DATA WITH $T_{ECC} \cong 212°F$ AND $J^*_{fin} = 0.12$ PLOTTED ON J* COORDINATES

Quick calculations using our hot wall model showed that even if it was assumed that all walls were initially at 300°F, the reduction in the complete bypass point was negligible. A small but perceptible effect was calculated near the complete delivery point, with heated walls requiring less steam flow for partial bypass. That is, when the walls are hot, the steam flux at the complete delivery point $J^*_{gc}$ is lower on a conventional plot of $J^*_{gc}$ as a function of $J^*_{fd}$. We anticipated a negligible calculated effect on complete delivery if correct (lower) wall temperatures and the correct (smaller) wall area were used. Rather than perform additional calculations, however, we performed a set of comparison tests.

In tests referred to here as "neutral" wall we preset the steam flow control valve to provide the desired test flow. Steam was bled into the vessel at a much lower rate such that the steam was at saturation temperature as it entered the vessel. Steam bleed was maintained for long periods to purge air and heat the entire vessel to saturation temperature, a result confirmed by wall surface thermocouples. The test is performed by initiating steam flow and ECC flow in rapid succession. Tests with this "neutral" wall procedure give penetration data in close agreement with the "heated" wall data as seen in Figure 1.

While we might do still more diagnosis to examine the potential wall temperature effects, we concluded that further effort was best deferred until the data had been analyzed. We prefer the "heated" wall procedure because it avoids the additional shock of sudden steam supply to the vessel. Therefore, the "heated" wall procedure was used in our remaining tests.

## 4 SUBCOOLED ECC DATA

Two ECC subcoolings have been tested for $J^*_{fin}$=0.12 at 1/5 scale. The higher subcooling is approximately 70°F (145°F ECC), and the lower subcooling is approximately 10-15°F in the range of partial to complete bypass.

The results of the highest subcooling are plotted in linear dimensionless coordinates in Figure 2a and in square-root coordinates in Figure 2b. The steam flow at which complete bypass occurs is somewhat higher than that for saturated ECC (also shown), as expected for this greater amount of subcooling.

The data with a low subcooling are shown in Figure 3, also in comparison with the saturated ECC data. From these figures it is observed that the limit for complete bypass is very similar in these two cases. The 205°F ECC data do show a tendency towards greater delivery at lower steam flows (towards the delivery end of the flooding curve). In fact, there is a tendency for the curve to "flatten out", that is, for there to be a large amount of scatter in the delivery data between large and small amounts of delivery at low steam flows.

As an illustration of the penetration behavior near complete delivery, Figure 4a is presented. These data show that even under steady inlet conditions of $J^*_{gc}$=0.05 the penetration curve may have a low slope at first and then increase in slope as time proceeds. This makes the interpretation of the filling rate difficult and can lead to the type of scatter shown in Figure 3a for the low and high (indicated by dashed symbol) filling rates at this steam flow. This effect is only observed at the lower steam flows with this low subcooling. Data obtained under all other conditions do not show this behavior and Figure 4b is entirely typical of the filling transients recorded in the great majority of the tests.

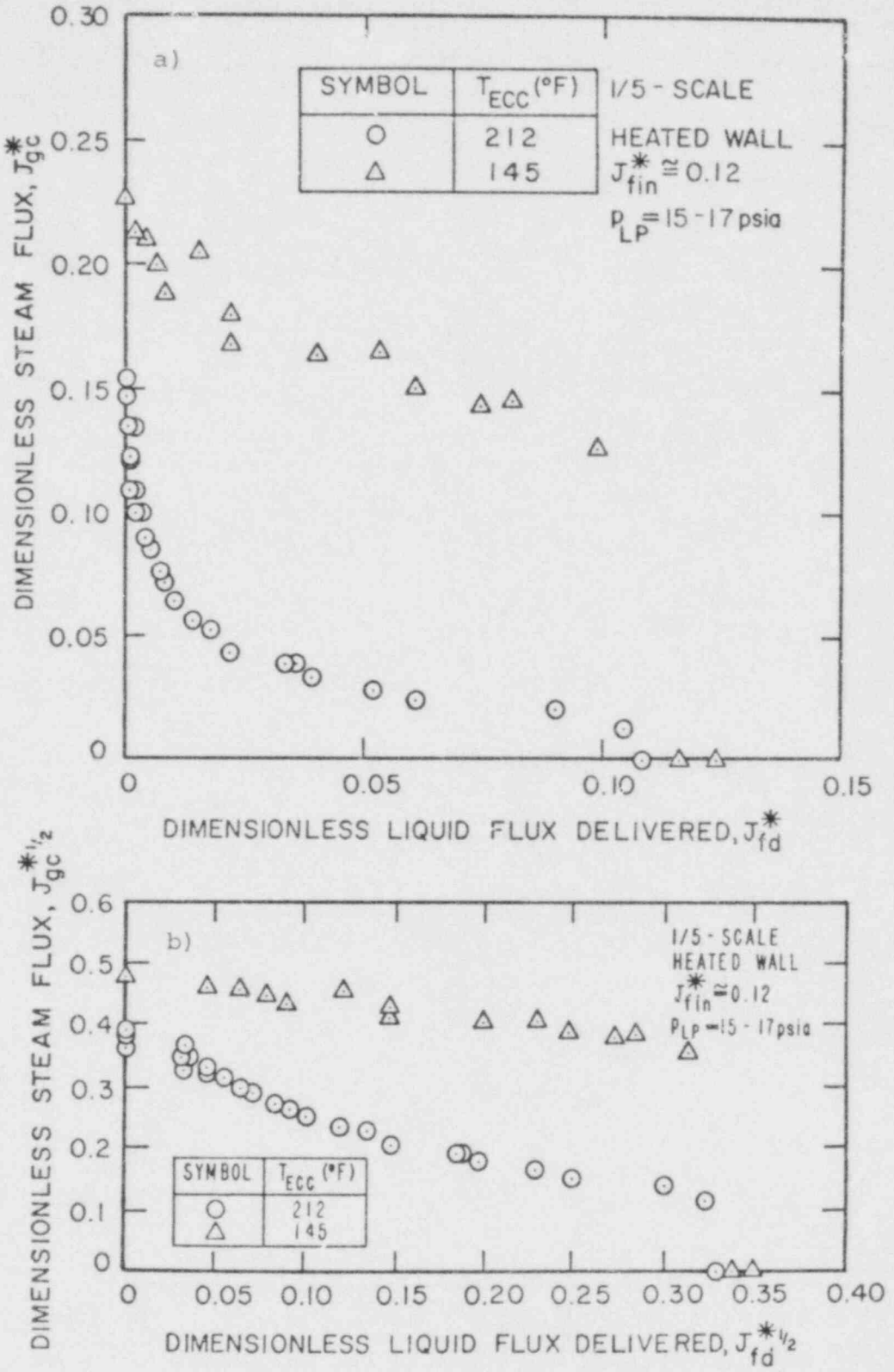


Figure 2. COMPARISON OF 1/5-SCALE CCF DATA WITH $T_{ECC} \cong 212°F$ AND $T_{ECC} \cong 145°F$ ($J^*_{fin} \cong 0.12$) PLOTTED ON J* COORDINATES

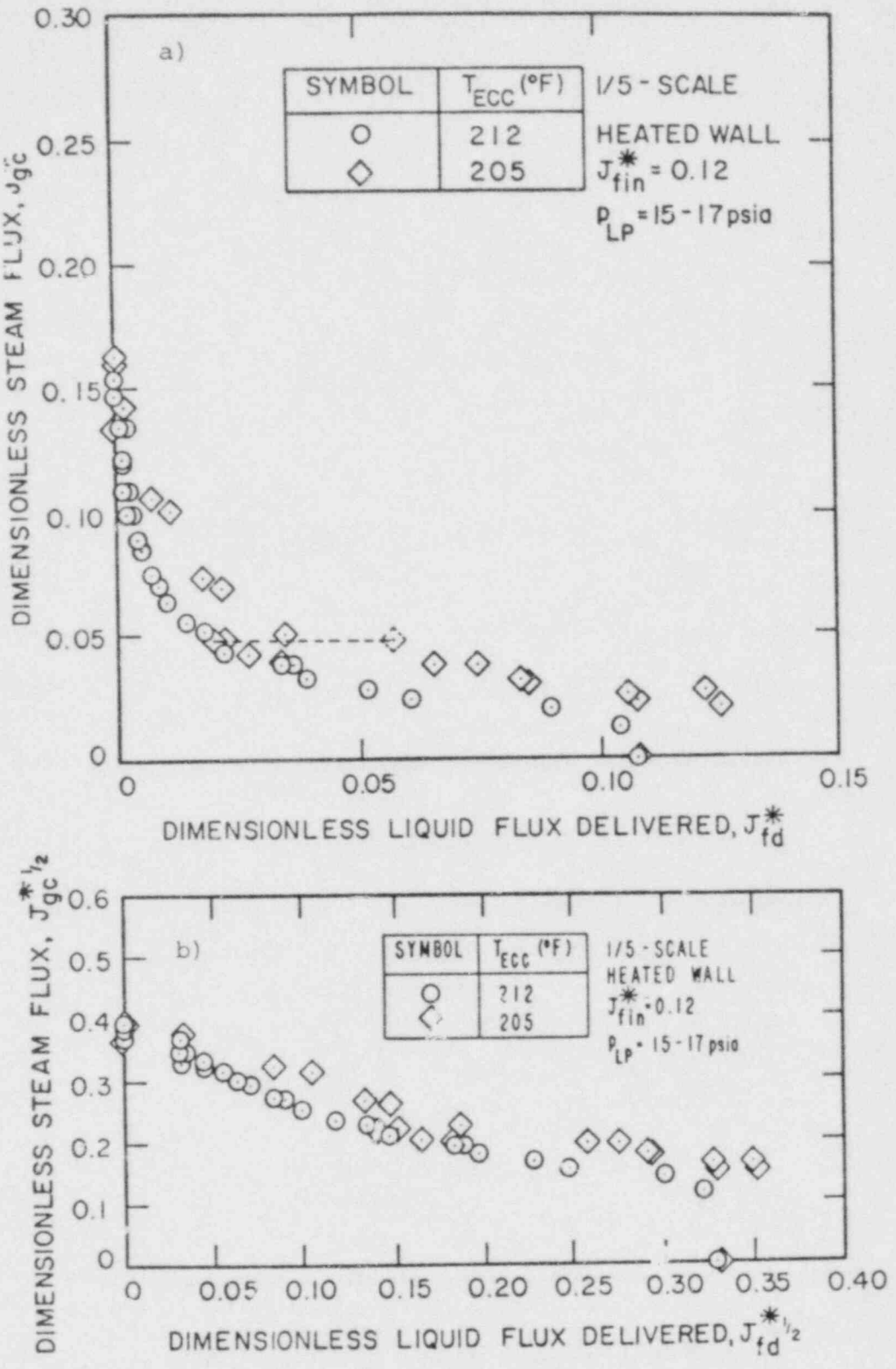


Figure 3. COMPARISON OF 1/5-SCALE CCF DATA WITH $T_{ECC} \approx 212°F$ AND $T_{ECC} \approx 205°F$ ($J^*_{fin} \approx 0.12$) PLOTTED ON J* COORDINATES

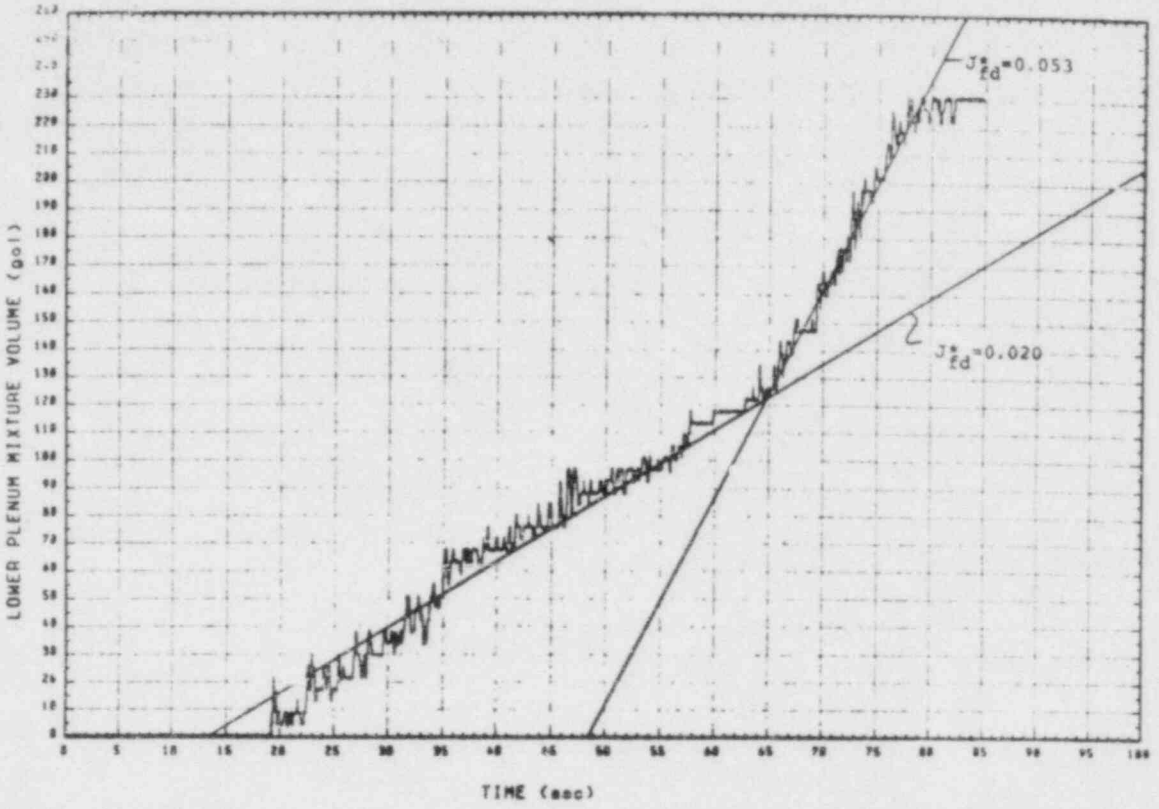


Figure 4a. UNUSUAL PLENUM FILLING DATA WITH $J^*_{gc} \simeq 0.05$, $T_{ECC} \simeq 205°F$ AND $J^*_{fin} \simeq 0.12$

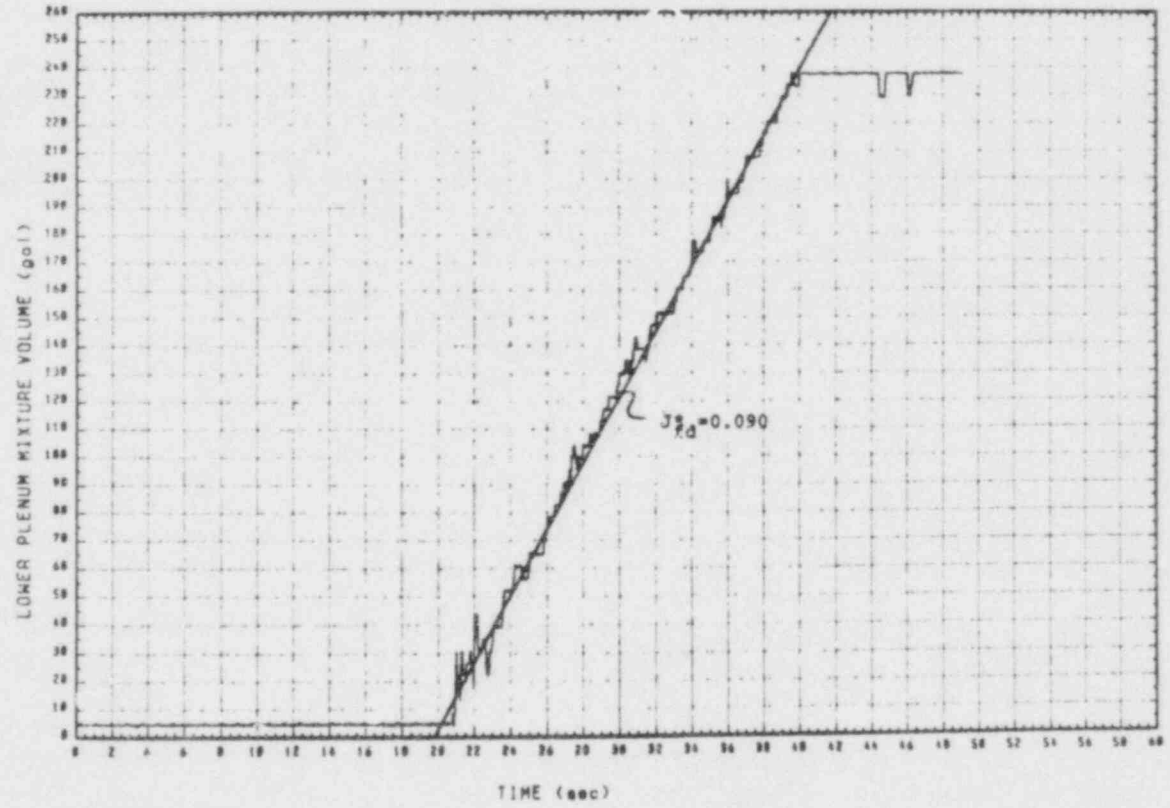


Figure 4b. TYPICAL PLENUM FILLING DATA WITH $J^*_{gc} \simeq 0.05$, $T_{ECC} \simeq 212°F$ AND $J^*_{fin} \simeq 0.12$

## 5 CREARE DATA COMPARISONS AND DISCUSSION

In Figures 5a and 5b Creare "saturated" ECC data from 1/30 [4], 1/15 [5], and 1/5 scales are compared on J* coordinates. There is a trend towards a lower bypass point (bypass intercept) as scale is increased. The statistical analysis in Appendix C indicates that complete bypass occurs at a steam flux $J^*_{gc}$=0.12 to 0.14 for 1/5 scale. This is less than at 1/15-scale where bypass occurs at approximately $J^*_{gc}$=0.15 to 0.18 (Figure C-2). The trend of these 1/5-scale data towards a lower bypass limit at large scale is consistent with constant momentum flux (or $J^*\sqrt{w}$) scaling of hydraulic phenomena and agrees with a trend previously indicated by 2/15-scale data.

There is also some variation in the slope of the penetration curve with scale. The slope effect is seen more easily in Figure 5b. The 1/30-scale data have a smaller slope than the data at larger scale. (In Figure 5a it is difficult to distinguish changes in slope of the penetration curve since the bypass point is difficult to pinpoint).

Figure 6 compares "saturated" ECC data at two scales for a lower injection rate, $J^*_{fin}$=0.06 [5]. The complete bypass point is ill-defined at 1/15-scale, though the bulk of the curve lies above the 1/5-scale data as for the larger flow rate shown in Figure 5.

Figure 7 compares subcooled ECC data at two scales. The 1/5-scale data lie slightly higher than the 1/15-scale data [2]. Coupled with the decrease in saturated ECC bypass point at large scale, this trend is indicative of an increase in the effect of condensation with increased scale. The statistical analysis in Appendix C shows that the condensation efficiency $f$ (a fraction of thermal equilibrium) increases from about 0.14 to 0.16 for Creare data at 1/15-scale to 0.2 to 0.3 at 1/5-scale (Figure C-3 or C-4).

For comparison the data of Figure 5 are replotted using $J^*\sqrt{S}$ coordinates in Figure 8. S is a scale factor determined by dividing the average annulus circumference in the model by that in the prototype. The relative positions of these sets of data are reversed thereby. The separation between the bulk of the penetration data appears smaller on these coordinates.

The dimensionless $J^*\sqrt{S}$ coordinates give similar results to the dimensionless Kutateladze parameter K* as shown by the coordinates on the right hand side of Figure 8. There is no basis, however, to prove or disprove the validity of the small surface tension effect in the K* parameter. The motivation behind the $J^*\sqrt{S}$ coordinates is to have a dimensionless parameter which has a similar effect to K*, but which does not imply that surface tension is a significant effect.

In Appendix A we describe our data reduction in detail and point out that steam densities are calculated at plenum conditions (saturated) for the preceding figures even though the inlet steam is superheated and its density is as much as 13% lower than saturated steam at plenum pressure. Qualitatively, lower densities at fixed (independently metered) mass flux give higher $J^*_{gc}$ by 3-6%. Thus, use of inlet steam density would tend to compress the data comparisons on Figure 5 and separate the data on Figure 8. This uncertainty is relatively small, however, and does not change the basic conclusions regarding these data.

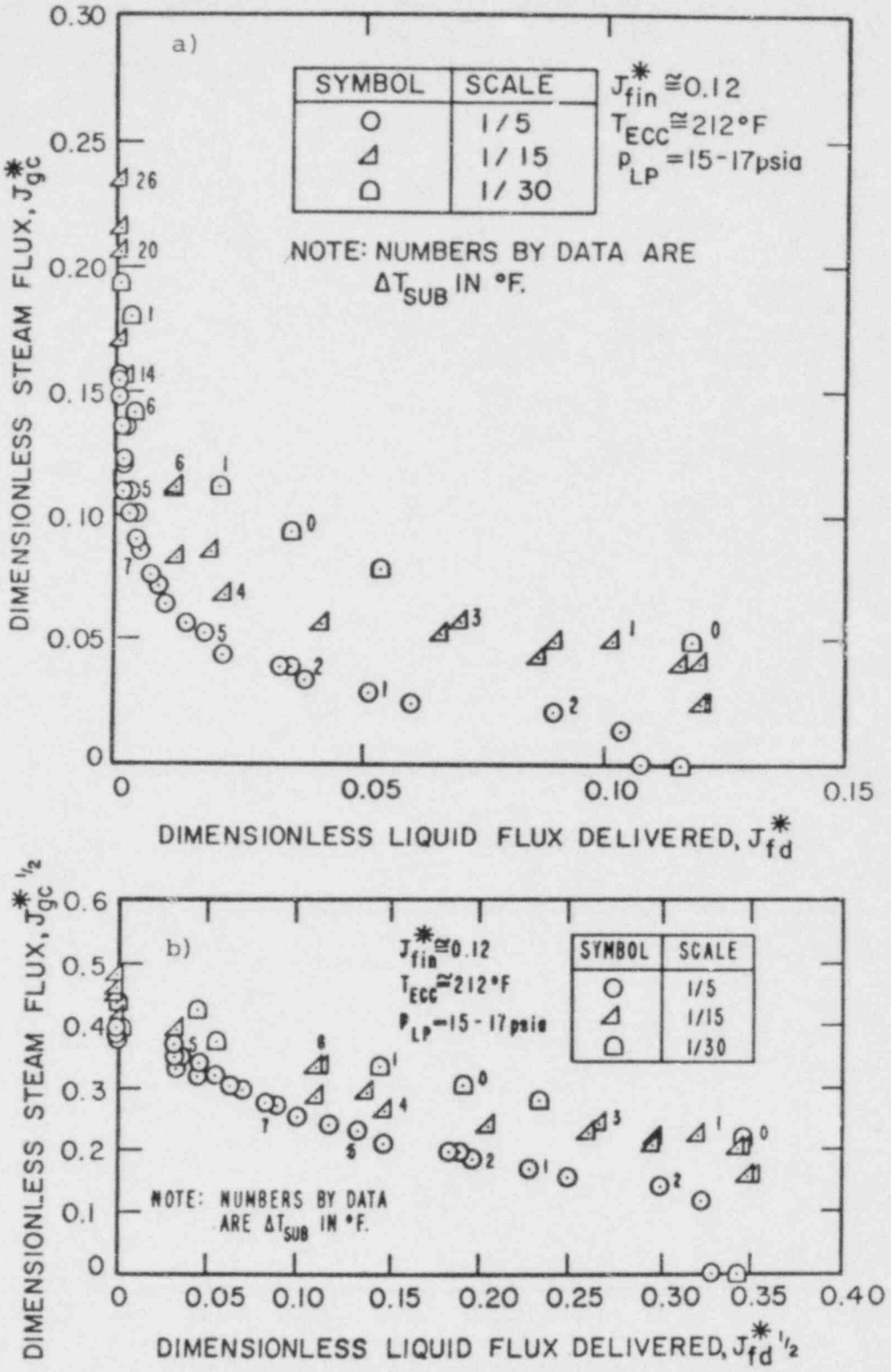


Figure 5. COMPARISON OF CCF DATA AT 1/5, 1/15, AND 1/30 SCALES WITH $T_{ECC} \cong 212°F$ AND $J^*_{fin} \cong 0.12$ PLOTTED ON J* COORDINATES

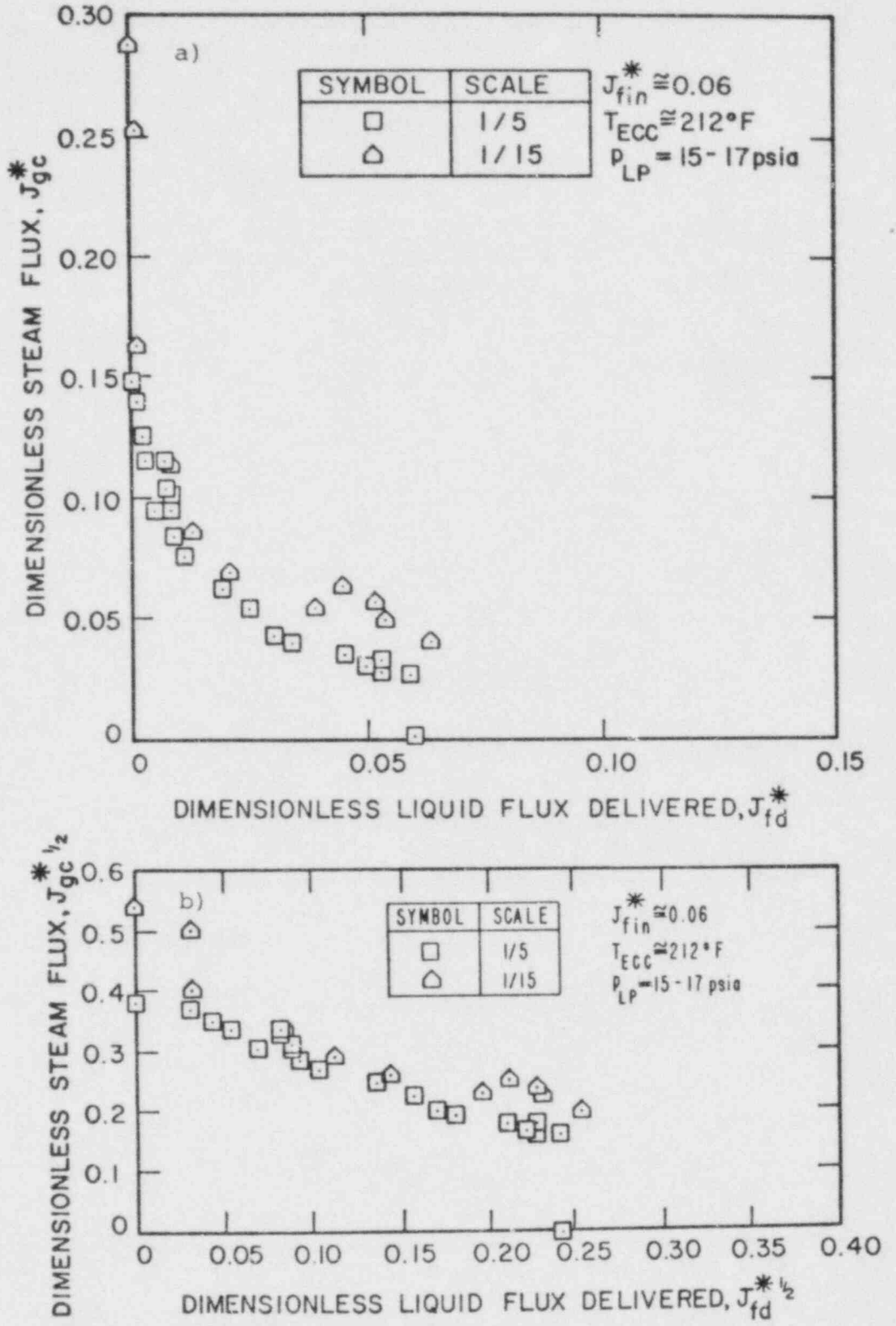


Figure 6. COMPARISON OF CCF DATA AT 1/5 AND 1/15 SCALES WITH $T_{ECC} \cong 212°F$ AND $J^*_{fin} \cong 0.06$ PLOTTED ON J* COORDINATES

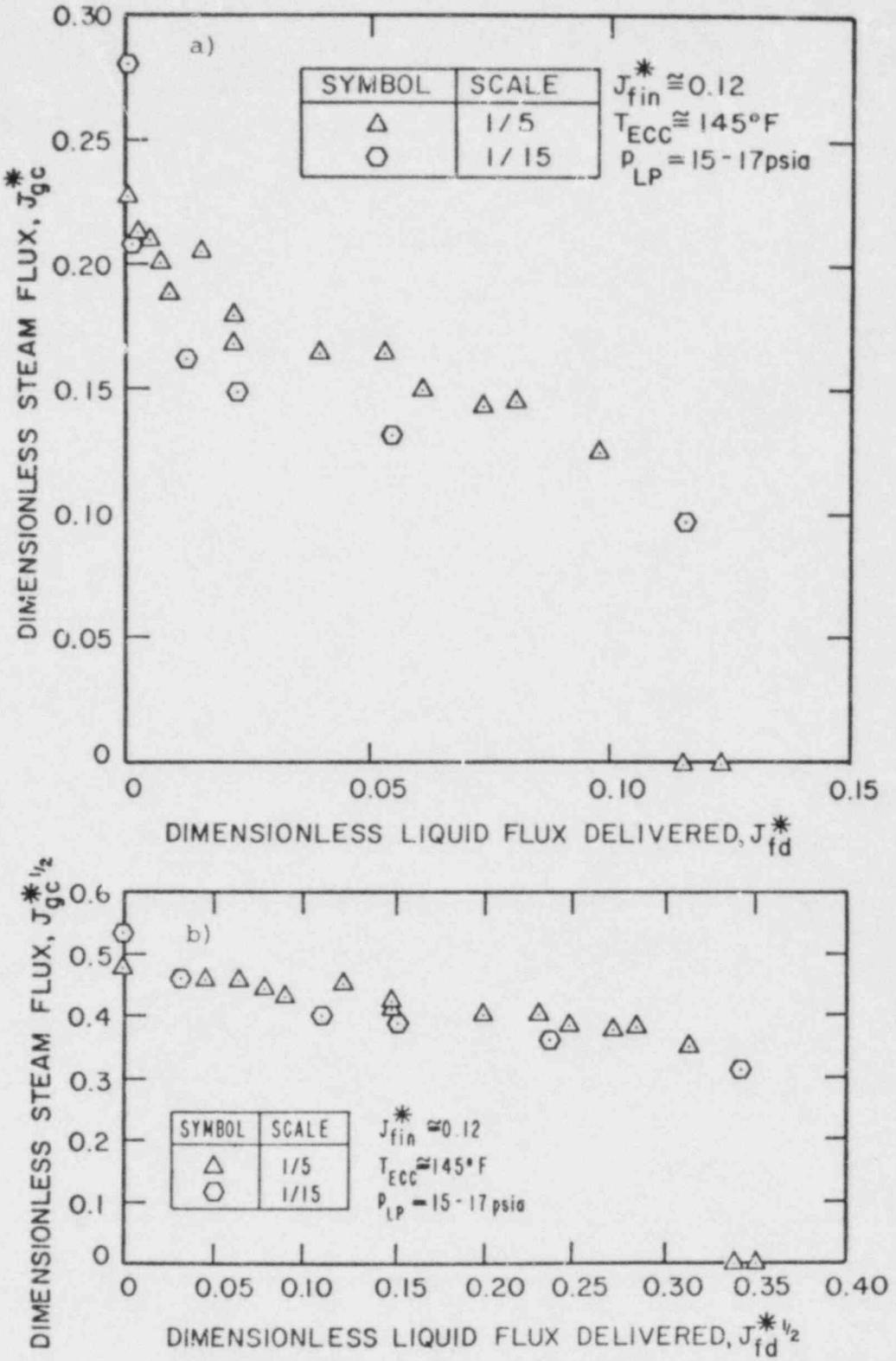


Figure 7. COMPARISON OF CCF DATA AT 1/5 AND 1/15 SCALES WITH $T_{ECC} \simeq 145°F$ AND $J^*_{fin} \simeq 0.12$ PLOTTED ON J* COORDINATES

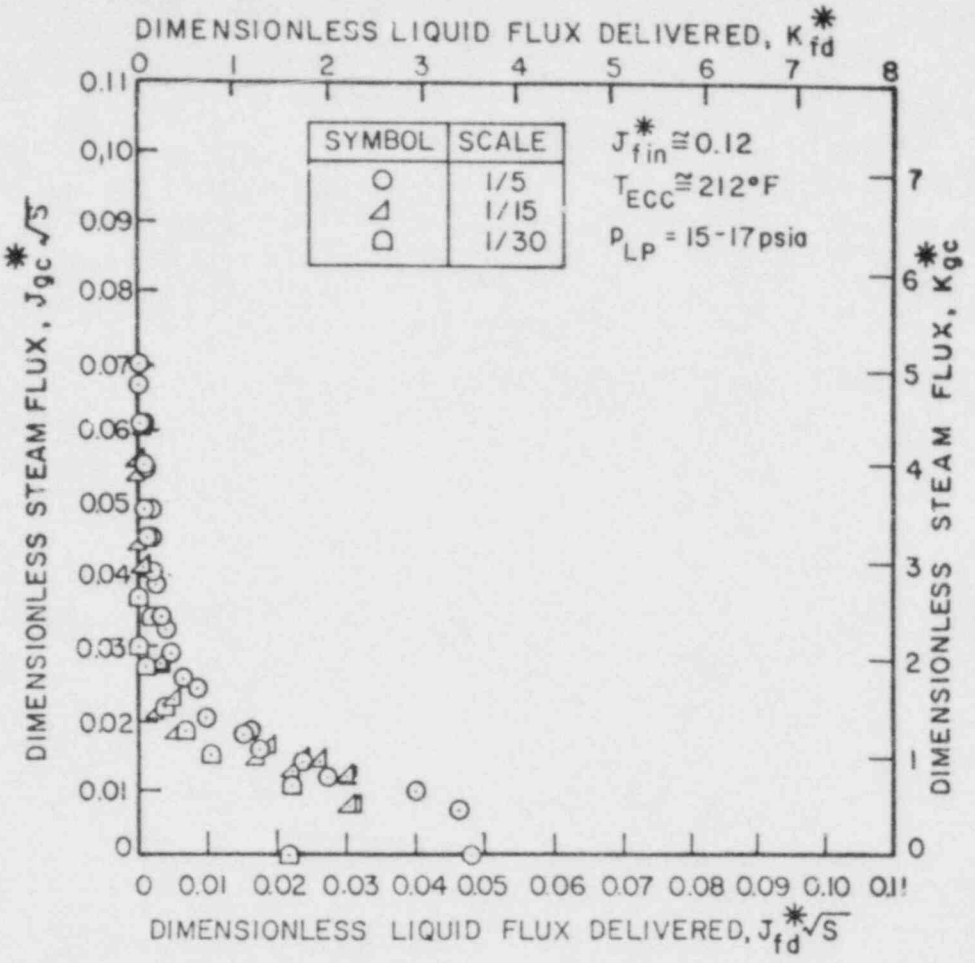


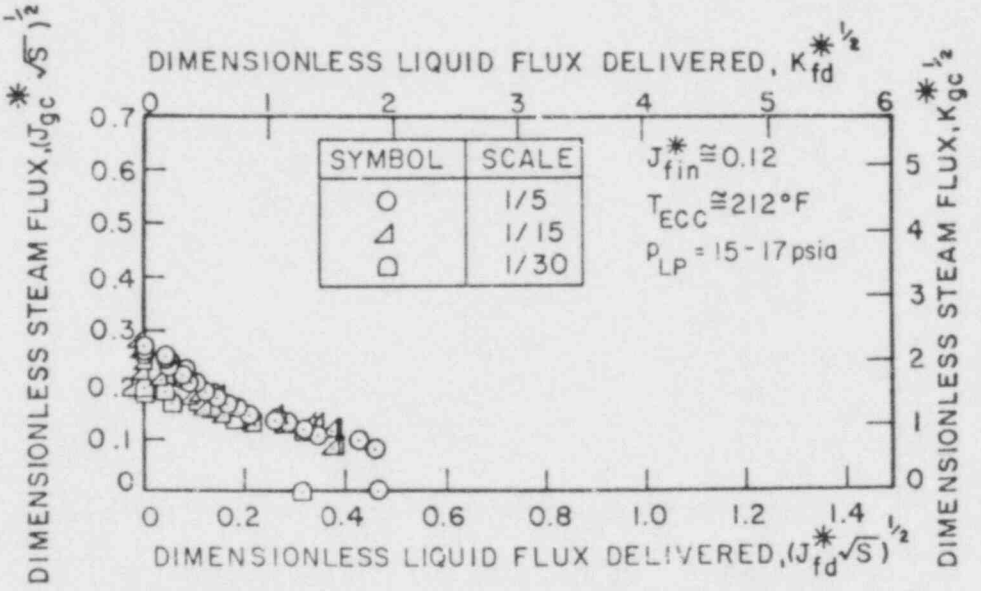


Figure 8. COMPARISON OF CCF DATA AT 1/5, 1/15, AND 1/30 SCALES WITH $T_{ECC} \cong 212°F$ AND $J^*_{fin} \cong 0.12$ PLOTTED ON K* COORDINATES

REFERENCES


1) Crowley, C. J. and Sam, R. G.: EXPERIMENTAL FACILITY AND TYPICAL RESULTS FOR FLASHING TRANSIENTS AT 1/5 SCALE; Creare Technical Memorandum TM-707, July 1980.

2) Rothe, P. H. and Crowley, C. J.; SCALING OF PRESSURE AND SUBCOOLING FOR COUNTERCURRENT FLOW; Quarterly Progress Report April 1 - June 30, 1978; Creare TN-285 (NUREG/CR-0464), October 1978.

3) Collier, R. P., et al.: STEAM-WATER MIXING AND SYSTEM HYDRODYNAMICS PROGRAM - TASK 4; Quarterly Progress Report July - September 1979, Battelle Columbus Labs. BMI-2058 (NUREG/CR-1625), August 1980.

4) C. J. Crowley letter to W. D. Beckner, January 11, 1979.

5) Rothe, P. H., Crowley, C. J. and Block, J. A.: PROGRESS ON ECC BYPASS SCALING; Quarterly Progress Report October 1 - December 31, 1977; Creare TN-272 (NUREG/CR-0048); March 1978.

6) Kline, S. J. and McClintock, F. A.; DESCRIBING UNCERTAINTIES IN SINGLE SAMPLE MEASUREMENTS; Mechanical Engrg., Vol. 75, No. 1, January 1953, pp. 3-9.

7) Bean, H. S.; FLUID METERS, THEIR THEORY AND APPLICATION; Report of ASME Research Committee on Fluid Meters, 6th Edition, The American Society of Mechanical Engineers, 1971.

8) Beckner, W. D., Reves, J. N., Jr. and Anderson, P.: ANALYSIS OF ECC BYPASS DATA", NUREG-0573, U.S. NRC, July 1979.

9) Segev, A. and Collier, R. P.: APPLICATION OF BATTELLE'S MECHANISTIC MODEL TO LOWER PLENUM REFILL; Topical Report, Battelle Columbus Laboratories, NUREG/CR-2030 (BMI-2077), March 1981.

## APPENDIX A

## DATA UNCERTAINTY ANALYSIS

The uncertainty analysis for the dimensionless steam and liquid flows can be developed from the mathematical expression for each phase

$$J_x^* = \left[ \frac{W_x}{\rho_x^{\frac{1}{2}} s w^{3/2} (g\Delta\rho)^{\frac{1}{2}}} \right]$$

where $W_x$ is the phase mass flow rate
$\rho_x$ is the phase density
$s$ is the annulus gap size
$w$ is the annulus circumference
$g$ is the constant acceleration of gravity
$\Delta\rho$ is the density difference between the fluid phases

According to the method of Kline and McKlintock [6] the uncertainty in the $J^*$ parameter is

$$\frac{\Delta J_x^*}{J_x^*} = \left[ \left(\frac{\Delta W_x}{W_x}\right)^2 + \left(\frac{3}{2}\frac{\Delta w}{x}\right)^2 + \left(\frac{\Delta s}{s}\right)^2 + \left(\frac{1}{2}\frac{\Delta \rho_x}{\rho_x}\right)^2 + \left(\frac{1}{2}\frac{\Delta(\rho_f-\rho_g)^2}{(\rho_f-\rho_g)}\right) \right]^{\frac{1}{2}}$$

The uncertainty in $(\rho_f-\rho_g)$ is negligible with respect to other parameters. The geometric uncertainties in w and s are the same for both phases and are 0.21% and 3.3%, respectively. The uncertainty equation then reduces to

$$\frac{\Delta J_x^*}{J_x^*} = \left[ \left(\frac{\Delta W_x}{W_x}\right)^2 + \left(\frac{1}{2}\frac{\Delta \rho_x}{\rho_x}\right)^2 + 0.001 \right]^{\frac{1}{2}}$$

and depends upon the flow rate and phase density uncertainties.

### Steam Flux

The steam flow rate, $W_{gc}$, was measured using an orifice meter designed according to ASME standards. The significant factors affecting the accuracy of the steam flow rate measurement are uncertainties in the discharge coefficient ($\leq 1\%$), the expansion factor ($\leq 0.75\%$), the orifice diameter ($\leq 0.5\%$), the steam density ($\leq 0.5\%$), and the orifice meter pressure drop ($\leq 8.5\%$). These uncertainties combine to give an uncertainty in $W_{gc}$ of $\pm 4.5\%$ as the worst case. There are also fluctuations in the measured pressure drop which result in an additional uncertainty in $W_{gc}$. This leads to an overall uncertainty in $W_{gc}$ of $\pm 5\%$.

In determining the steam density to be used in the calculation, we have assumed the density for saturation conditions at the lower plenum pressure. This is because plenum temperatures tend to be at saturation as measured by plenum thermocouples (as long as the thermocouples are not submerged in delivered liquid). A typical plenum thermocouple measurement for a test near complete bypass in Figure 2 is shown in Figure A-1. Thermocouple measurements in the steam inlet line show, however, that the steam may be superheated to 300°F as it enters the vessel (Figure A-2), resulting in a possible 13% decrease in steam density. This would lead to a possible systematic trend in the $J^*_{gc}$ calculation for lower values compared with the values based on density at saturation. In either case, the density calculation itself has an uncertainty of ±1%. Values on $J^*_{gc}$ based on both densities are listed in the data tables of Appendix B.

Combining all of these uncertainties leads to a possible uncertainty of 9% in the direction of greater $J^*_{gc}$ and 6% in the direction of reduced $J^*_{gc}$. In this assessment the possible effect of steam superheat on steam density is treated as an uncertainty.

## Liquid Flux

For the uncertainty in the delivered liquid flux, the delivery rate measured by the conductivity probes is estimated at about 5% of the injected rate. The uncertainty in the liquid density is small, estimated at 2% at the most. Combining these uncertainties, the accuracy of the delivered flow rate is 5.4% of the injected flow rate. It is important to note that this uncertainty does not taken into account special effects such as shown in Figure 4 where the filling rate changes with time.

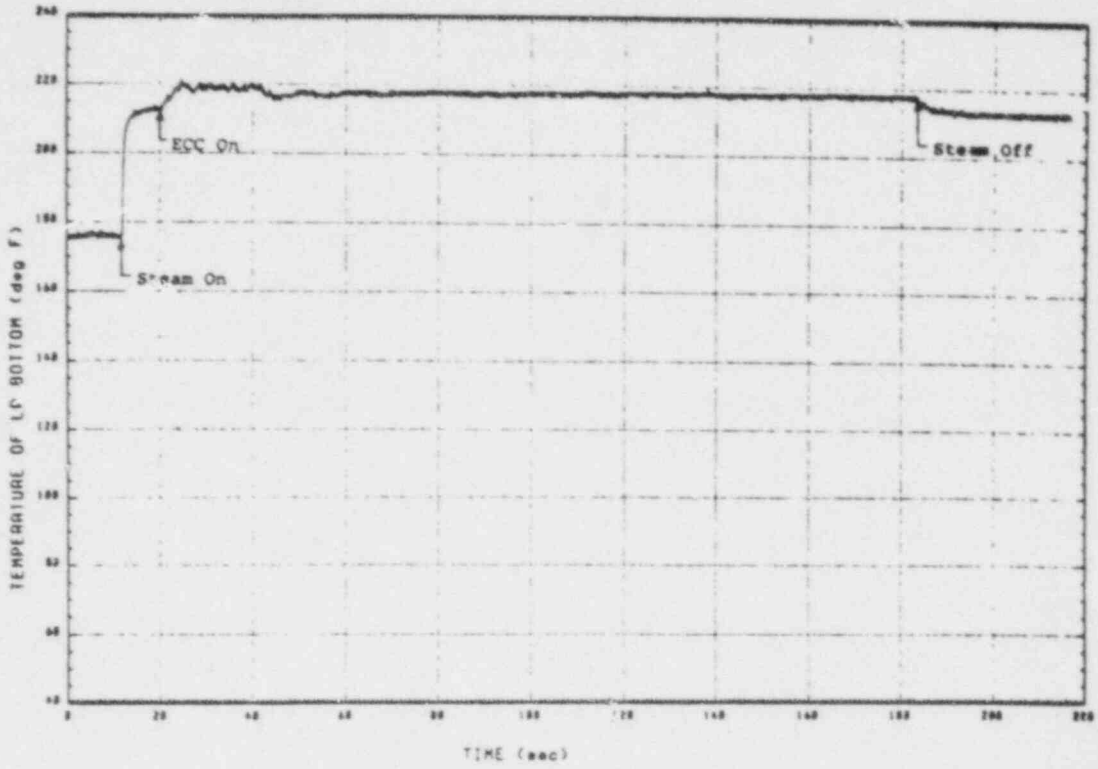


Figure A-1. LOWER PLENUM FLUID TEMPERATURE FOR A TYPICAL CCF TEST

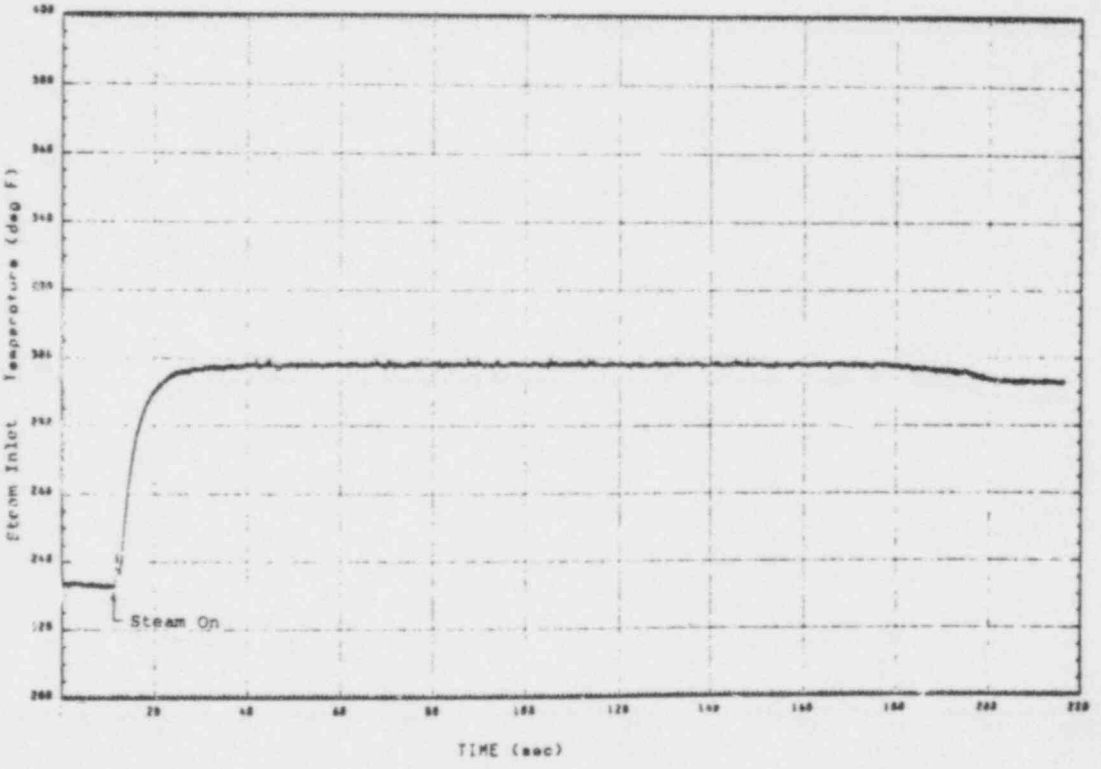


Figure A-2. TEMPERATURE OF STEAM ENTERING VESSEL FOR A TYPICAL CCF TEST

## APPENDIX B

## 1/5-SCALE CCF DATA TABULATION

This appendix contains all Creare 1/5-scale CCF data. The correspondence between test conditions and data table is given below.

TABLE B-1
NOMINAL TEST CONDITIONS FOR CREARE 1/5-SCALE CCF DATA

| Table | $J^*_{fin}$ | $T_{ECC}$ (°F) | Wall |
|---|---|---|---|
| B1 | 0.12 | 212 | Heated |
| B2 | 0.12 | 212 | Neutral |
| B3 | 0.06 | 212 | Heated |
| B4 | 0.06 | 212 | Neutral |
| B5 | 0.12 | 145 | Heated |
| B6 | 0.12 | 205 | Heated |

The information provided in the data tables includes

Test ID - identification number for each test

$Q_{fd}$ - volumetric water flow rate delivered to lower plenum, gpm

$Q_{fin}$ - volumetric water flow rate delivered into cold legs, gpm

$T_{ECC}$ - injected water temperature, °F

$\Delta T_{sub}$ - injected water subcooling, °F

$p_{LP}$ - lower plenum pressure, psia

$\rho_g$ - saturated steam density at lower plenum pressure, $lbm/ft^3$

$T_{in}$ - steam inlet temperature, °F*

$T_{sat}$ - saturation temperature, °F

$J^*_{fin}$ - dimensionless water flow rate injected

$J^*_{gc}$ - dimensionless countercurrent steam flow rate based on saturated steam density ($\rho_{gsat}$) at plenum pressure

$J^*_{fd}$ - dimensionless water flow rate delivered to lower plenum

$K^*_{fin}$ - dimensionless water flow rate injected

$K^*_{gc}$ - dimensionless countercurrent steam flow rate based on saturated steam density at lower plenum pressure

$h_{fg}$ - saturated steam latent heat at lower plenum pressure, Btu/lbm

*Bracketted values in the table mean that inlet temperature has been estimated. Actual data are not available.

$K^*_{fd}$ - dimensionless water flow rate delivered to lower plenum

$J^*_{gc(sup)}$ - dimensionless countercurrent steam flow rate based on steam inlet temperature and plenum pressure

$W_{gc}$ - countercurrent steam flow rate, lbm/sec

The dimensionless variables are defined by

$$J^*_x = \frac{W_x}{\rho_x^{\frac{1}{2}} (sw) [gw\Delta\rho]^{\frac{1}{2}}}$$

and

$$K^*_x = \frac{W_x}{\rho_x^{\frac{1}{2}} (sw) [g\sigma\Delta\rho]^{\frac{1}{4}}}$$

where $\sigma$ (surface tension) is given by the expression used in the RELAP4 code

$$\sigma = (700-T_{sat})x8.333x10^{-6} \text{ lb}_f/\text{ft}$$

The geometrical parameters are gap size s=1.5 in. and annulus circumference w=105.6 in.

In Figure 8 we have also used $J^*\sqrt{S}$ parameters which are defined as $J^*_x$ above, multiplied by $\sqrt{S}$ where $S = \text{model}/\text{prototype}$. The factor S=0.207 for these 1/5-scale experiments. All $J^*_x$ numbers in the following tables should be multiplied by $(0.207)^{\frac{1}{2}}=0.455$ to obtain the values plotted in Figure 8 in terms of $J^*\sqrt{S}$.

TABLE B1

| Test | Qfd (gpm) | Qfin (gpm) | Tecc (F) | DTsub (F) | Plp (psia) | RHOg (#/FT3) | Tin (F) | Tsat (F) | J*fin | J*gc | J*fd | K*fin | K*gc | K*fd | J*gc (sup) | Wgc (#/sec) | Hfg (BTU/#) |
|---|---|---|---|---|---|---|---|---|---|---|---|---|---|---|---|---|---|
| 2.5047 | 70 | 990 | 210 | 6 | 16.0 | 0.040 | 290 | 216 | 0.119 | 0.071 | 0.008 | 3.897 | 2.325 | 0.262 | 0.075 | 2.06 | 967.6 |
| 2.5048 | 9 | 950 | 210 | 9 | 16.7 | 0.042 | 290 | 218 | 0.114 | 0.122 | 0.001 | 3.737 | 3.959 | 0.033 | 0.128 | 3.58 | 966.2 |
| 2.5049 | 10 | 950 | 207 | 11 | 16.7 | 0.042 | 290 | 218 | 0.114 | 0.135 | 0.001 | 3.737 | 4.426 | 0.033 | 0.142 | 4.00 | 966.2 |
| 2.5050 | 18 | 950 | 211 | 7 | 16.5 | 0.042 | 290 | 218 | 0.114 | 0.100 | 0.002 | 3.736 | 3.277 | 0.066 | 0.105 | 2.94 | 966.6 |
| 2.5051 | 153 | 875 | 210 | 5 | 15.5 | 0.039 | 290 | 215 | 0.105 | 0.052 | 0.018 | 3.437 | 1.702 | 0.589 | 0.055 | 1.48 | 968.7 |
| 2.5052 | 0 | 990 | 211 | 8 | 17.0 | 0.043 | 290 | 219 | 0.119 | 0.154 | 0.000 | 3.901 | 5.049 | 0.000 | 0.162 | 4.58 | 965.6 |
| 2.5053 | 297 | 960 | 210 | 5 | 15.3 | 0.039 | 290 | 214 | 0.115 | 0.038 | 0.036 | 3.762 | 1.243 | 1.178 | 0.040 | 1.06 | 969.1 |
| 2.5054 | 0 | 925 | 213 | 6 | 17.2 | 0.043 | 290 | 220 | 0.111 | 0.147 | 0.000 | 3.641 | 4.822 | 0.000 | 0.154 | 4.40 | 965.2 |
| 2.5055 | 433 | 910 | 210 | 3 | 14.9 | 0.038 | 290 | 213 | 0.109 | 0.028 | 0.052 | 3.564 | 0.916 | 1.700 | 0.030 | 0.80 | 969.9 |
| 2.5056 | 865 | 915 | 211 | 1 | 14.6 | 0.037 | 290 | 212 | 0.110 | 0.013 | 0.104 | 3.593 | 0.425 | 3.397 | 0.014 | 0.38 | 970.5 |
| 2.5057 | 750 | 935 | 210 | 2 | 14.8 | 0.038 | 290 | 213 | 0.112 | 0.020 | 0.090 | 3.662 | 0.654 | 2.943 | 0.021 | 0.56 | 970.1 |
| 2.5058 | 511 | 960 | 211 | 1 | 14.9 | 0.038 | 290 | 213 | 0.113 | 0.024 | 0.061 | 3.693 | 0.784 | 1.994 | 0.025 | 0.66 | 969.9 |
| 2.5059 | 960 | 980 | 210 | 2 | 14.5 | 0.037 | 290 | 211 | 0.118 | 0.000 | 0.108 | 3.854 | 0.000 | 3.528 | 0.000 | 0.00 | 970.7 |
| 2.5074 | 11 | 860 | 213 | 5 | 16.6 | 0.042 | 290 | 218 | 0.103 | 0.109 | 0.001 | 3.375 | 3.572 | 0.033 | 0.115 | 3.20 | 966.4 |
| 2.5075 | 35 | 870 | 213 | 4 | 16.3 | 0.041 | 290 | 217 | 0.104 | 0.089 | 0.004 | 3.406 | 2.915 | 0.131 | 0.094 | 2.56 | 967.0 |
| 2.5076 | 84 | 885 | 213 | 3 | 16.0 | 0.040 | 290 | 216 | 0.106 | 0.064 | 0.010 | 3.470 | 2.095 | 0.327 | 0.067 | 1.82 | 967.6 |
| 2.5077 | 181 | 895 | 212 | 3 | 15.5 | 0.039 | 290 | 215 | 0.107 | 0.043 | 0.022 | 3.501 | 1.407 | 0.720 | 0.045 | 1.24 | 968.7 |
| 2.5078 | 323 | 910 | 211 | 2 | 15.1 | 0.038 | 290 | 215 | 0.109 | 0.033 | 0.039 | 3.566 | 1.080 | 1.276 | 0.035 | 0.93 | 969.5 |
| 2.5084 | 0 | 910 | 212 | 8 | 17.2 | 0.043 | 290 | 220 | 0.109 | 0.135 | 0.000 | 3.575 | 4.428 | 0.000 | 0.142 | 4.05 | 965.2 |
| 2.5085 | 6 | 900 | 212 | 7 | 16.8 | 0.042 | 290 | 218 | 0.108 | 0.120 | 0.001 | 3.539 | 3.932 | 0.033 | 0.126 | 3.38 | 966.0 |
| 2.5086 | 13 | 900 | 212 | 6 | 16.7 | 0.042 | 290 | 218 | 0.108 | 0.109 | 0.002 | 3.539 | 3.572 | 0.066 | 0.115 | 3.15 | 966.2 |
| 2.5087 | 28 | 885 | 212 | 6 | 16.5 | 0.042 | 290 | 218 | 0.106 | 0.100 | 0.003 | 3.473 | 3.277 | 0.098 | 0.105 | 2.92 | 966.6 |
| 2.5088 | 71 | 850 | 213 | 5 | 16.2 | 0.041 | 290 | 217 | 0.102 | 0.075 | 0.007 | 3.341 | 2.456 | 0.229 | 0.079 | 2.17 | 967.2 |
| 2.5089 | 113 | 890 | 211 | 5 | 15.8 | 0.040 | 290 | 215 | 0.107 | 0.056 | 0.014 | 3.501 | 1.832 | 0.458 | 0.059 | 1.60 | 968.0 |
| 2.5090 | 283 | 900 | 210 | 4 | 15.3 | 0.039 | 290 | 214 | 0.108 | 0.038 | 0.034 | 3.533 | 1.243 | 1.112 | 0.040 | 1.05 | 969.1 |
| 2.5092 | 45 | 960 | 210 | 7 | 16.3 | 0.041 | 290 | 217 | 0.115 | 0.085 | 0.005 | 3.768 | 2.785 | 0.164 | 0.089 | 2.32 | 967.0 |

TABLE B2

| Test | Qfd (gpm) | Qfin (gpm) | Tecc (F) | DTsub (F) | Plp (psia) | RHOg (#/FT3) | Tin (F) | Tsat (F) | J*fin | J*gc | J*fd | K*fin | K*gc | K*fd | J*gc (sup) | Wgc (#/sec) | Hfg (BTU/#) |
|---|---|---|---|---|---|---|---|---|---|---|---|---|---|---|---|---|---|
| 2.5104 | 26 | 890 | 213 | 5 | 16.5 | 0.042 | 298 | 218 | 0.107 | 0.090 | 0.003 | 3.506 | 2.949 | 0.098 | 0.095 | 2.62 | 966.6 |
| 2.5105 | 10 | 910 | 212 | 6 | 16.5 | 0.042 | 292 | 218 | 0.109 | 0.101 | 0.001 | 3.572 | 3.310 | 0.033 | 0.106 | 3.05 | 966.6 |
| 2.5106 | 0 | 890 | 211 | 7 | 16.7 | 0.042 | 292 | 218 | 0.107 | 0.116 | 0.000 | 3.506 | 3.801 | 0.000 | 0.122 | 3.32 | 966.2 |
| 2.5107 | 48 | 880 | 212 | 5 | 16.3 | 0.041 | 302 | 217 | 0.106 | 0.073 | 0.006 | 3.472 | 2.391 | 0.197 | 0.077 | 2.08 | 967.0 |
| 2.5108 | 133 | 885 | 212 | 3 | 15.7 | 0.040 | 292 | 215 | 0.106 | 0.046 | 0.016 | 3.468 | 1.505 | 0.523 | 0.049 | 1.31 | 968.2 |
| 2.5109 | 208 | 880 | 212 | 2 | 15.4 | 0.039 | 283 | 214 | 0.106 | 0.059 | 0.025 | 3.466 | 1.929 | 0.818 | 0.062 | 1.15 | 968.9 |
| 2.5110 | 383 | 855 | 209 | 4 | 15.0 | 0.038 | 304 | 213 | 0.103 | 0.029 | 0.046 | 3.368 | 0.948 | 1.504 | 0.031 | 0.81 | 969.7 |
| 2.5111 | 567 | 825 | 212 | 0 | 14.9 | 0.038 | 295 | 213 | 0.099 | 0.022 | 0.068 | 3.236 | 0.719 | 2.223 | 0.023 | 0.61 | 969.9 |
| 2.5113 | 279 | 910 | 211 | 3 | 15.3 | 0.039 | 293 | 214 | 0.109 | 0.035 | 0.033 | 3.564 | 1.145 | 1.079 | 0.037 | 0.98 | 969.1 |
| 2.5114 | 517 | 910 | 211 | 2 | 15.0 | 0.038 | 280 | 213 | 0.109 | 0.026 | 0.062 | 3.563 | 0.850 | 2.026 | 0.027 | 0.71 | 969.7 |
| 2.5115 | 758 | 885 | 212 | 0 | 14.7 | 0.037 | 312 | 212 | 0.106 | 0.013 | 0.091 | 3.463 | 0.425 | 2.973 | 0.014 | 0.37 | 970.3 |
| 2.5116 | 0 | 845 | 210 | 8 | 16.8 | 0.042 | 300 | 218 | 0.101 | 0.121 | 0.000 | 3.311 | 3.967 | 0.000 | 0.128 | 3.66 | 966.0 |
| 2.5117 | 92 | 870 | 212 | 4 | 16.0 | 0.040 | 293 | 216 | 0.104 | 0.061 | 0.011 | 3.404 | 1.997 | 0.360 | 0.064 | 1.78 | 967.6 |

TABLE B3

| Test | Qfd (gpm) | Qfin (gpm) | Tecc (F) | DTsub (F) | Plp (psia) | RHOg (#/FT3) | Tin (F) | Tsat (F) | J*fin | J*gc | J*fd | K*fin | K*gc | K*fd | J*gc (sup) | wgc (#/sec) | Hfg (BTU/#) |
|---|---|---|---|---|---|---|---|---|---|---|---|---|---|---|---|---|---|
| 2.5032 | 69 | 510 | 214 | 2 | 16.0 | 0.040 | 290 | 216 | 0.061 | 0.095 | 0.008 | 1.997 | 3.110 | 0.262 | 0.100 | 2.70 | 967.6 |
| 2.5033 | 37 | 450 | 215 | 1 | 16.0 | 0.040 | 290 | 216 | 0.054 | 0.094 | 0.005 | 1.767 | 3.076 | 0.164 | 0.099 | 2.70 | 967.6 |
| 2.5034 | 206 | 475 | 213 | 0 | 15.0 | 0.038 | 290 | 213 | 0.057 | 0.053 | 0.025 | 1.863 | 1.732 | 0.817 | 0.056 | 1.48 | 969.7 |
| 2.5035 | 13 | 450 | 216 | 2 | 16.5 | 0.042 | 290 | 218 | 0.054 | 0.125 | 0.002 | 1.769 | 4.094 | 0.066 | 0.131 | 3.70 | 966.6 |
| 2.5036 | 254 | 450 | 210 | 3 | 15.0 | 0.038 | 290 | 213 | 0.054 | 0.042 | 0.030 | 1.766 | 1.373 | 0.981 | 0.044 | 1.15 | 969.7 |
| 2.5037 | 440 | 520 | 211 | 1 | 14.7 | 0.037 | 290 | 212 | 0.062 | 0.028 | 0.053 | 2.025 | 0.915 | 1.731 | 0.030 | 0.80 | 970.3 |
| 2.5038 | 499 | 520 | 208 | 4 | 14.5 | 0.037 | 290 | 211 | 0.062 | 0.000 | 0.060 | 2.025 | 0.000 | 1.960 | 0.000 | 0.00 | 970.7 |
| 2.5039 | 492 | 530 | 210 | 1 | 14.5 | 0.037 | 290 | 211 | 0.064 | 0.026 | 0.059 | 2.090 | 0.849 | 1.926 | 0.027 | 0.70 | 970.7 |
| 2.5040 | 280 | 510 | 213 | 0 | 15.0 | 0.038 | 290 | 213 | 0.061 | 0.039 | 0.034 | 1.994 | 1.275 | 1.111 | 0.041 | 1.09 | 969.7 |
| 2.5041 | 77 | 520 | 213 | 2 | 15.5 | 0.039 | 290 | 215 | 0.062 | 0.083 | 0.009 | 2.028 | 2.716 | 0.294 | 0.087 | 2.37 | 968.7 |
| 2.5042 | 24 | 500 | 211 | 5 | 16.0 | 0.040 | 290 | 216 | 0.060 | 0.115 | 0.003 | 1.964 | 3.764 | 0.098 | 0.121 | 3.35 | 967.6 |
| 2.5043 | 0 | 530 | 214 | 4 | 16.5 | 0.042 | 290 | 218 | 0.064 | 0.148 | 0.000 | 2.097 | 4.850 | 0.000 | 0.156 | 4.35 | 966.6 |
| 2.5044 | 5 | 520 | 215 | 3 | 16.5 | 0.042 | 290 | 218 | 0.062 | 0.140 | 0.001 | 2.031 | 4.586 | 0.033 | 0.147 | 4.12 | 966.6 |
| 2.5045 | 60 | 530 | 213 | 2 | 15.5 | 0.039 | 290 | 215 | 0.064 | 0.062 | 0.019 | 2.094 | 2.028 | 0.622 | 0.065 | 1.75 | 968.7 |
| 2.5046 | 440 | 520 | 212 | 0 | 14.8 | 0.038 | 290 | 212 | 0.062 | 0.032 | 0.053 | 2.025 | 1.045 | 1.731 | 0.034 | 0.90 | 970.1 |
| 2.5071 | 56 | 580 | 214 | 1 | 15.5 | 0.039 | 290 | 215 | 0.070 | 0.115 | 0.007 | 2.290 | 3.763 | 0.229 | 0.121 | 3.35 | 968.7 |
| 2.5072 | 92 | 490 | 213 | 1 | 15.7 | 0.040 | 290 | 215 | 0.059 | 0.074 | 0.011 | 1.930 | 2.421 | 0.360 | 0.078 | 2.10 | 968.2 |
| 2.5073 | 417 | 540 | 212 | 0 | 14.7 | 0.037 | 290 | 212 | 0.065 | 0.030 | 0.050 | 2.123 | 0.980 | 1.633 | 0.032 | 0.82 | 970.3 |
| 2.5079 | 372 | 590 | 214 | 0 | 14.[illegible] | 0.038 | 290 | 213 | 0.071 | 0.034 | 0.045 | 2.321 | 1.111 | 1.471 | 0.036 | 0.94 | 969.9 |
| 2.5080 | 67 | 580 | 215 | 0 | 15.[illegible] | 0.039 | 290 | 213 | 0.070 | 0.100 | 0.008 | 2.287 | 3.267 | 0.261 | 0.106 | 2.90 | 969.3 |
| **2.5081** | **59** | **570** | **216** | **0** | **15.3** | **0.039** | **290** | **214** | **0.068** | **0.103** | **0.007** | **2.223** | **3.367** | **0.229** | **0.109** | **3.00** | **969.1** |

TABLE B4

| Test | Qfd (gpm) | Qfin (gpm) | Tecc (F) | DTsub (F) | Plp (psia) | RHOg (#/FT3) | Tin (F) | Tsat (F) | J*fin | J*gc | J*fd | K*fin | K*gc | K*fd | J*gc (sup) | wgc (#/sec) | Hfg (BTU/#) |
|---|---|---|---|---|---|---|---|---|---|---|---|---|---|---|---|---|---|
| 2.5122 | 123 | 600 | 216 | 0 | 16.0 | 0.040 | 295 | 216 | 0.072 | 0.072 | 0.015 | 2.356 | 2.356 | 0.491 | 0.076 | 2.05 | 967.6 |
| 2.5123 | 83 | 615 | 215 | 1 | 16.3 | 0.041 | 300 | 217 | 0.074 | 0.092 | 0.010 | 2.423 | 3.012 | 0.327 | 0.097 | 2.66 | 967.0 |
| 2.5124 | 267 | 500 | 213 | 0 | 15.0 | 0.038 | 290 | 213 | 0.060 | 0.050 | 0.032 | 1.961 | 1.634 | 1.046 | 0.053 | 1.39 | 969.7 |
| 2.5125 | 73 | 620 | 216 | 2 | 16.5 | 0.042 | 292 | 218 | 0.074 | 0.106 | 0.009 | 2.424 | 3.472 | 0.295 | 0.112 | 3.08 | 966.6 |
| 2.5126 | 53 | 625 | 215 | 3 | 16.5 | 0.042 | 292 | 218 | 0.075 | 0.119 | 0.006 | 2.457 | 3.898 | 0.197 | 0.125 | 3.50 | 966.6 |
| 2.5127 | 45 | 610 | 215 | 3 | 16.7 | 0.042 | 287 | 218 | 0.073 | 0.128 | 0.005 | 2.391 | 4.193 | 0.164 | 0.134 | 3.76 | 966.2 |
| 2.5128 | 367 | 615 | 212 | 1 | 15.0 | 0.038 | 275 | 213 | 0.074 | 0.041 | 0.044 | 2.419 | 1.340 | 1.438 | 0.043 | 1.14 | 969.7 |
| 2.5129 | 417 | 515 | 212 | 0 | 14.8 | 0.038 | 240 | 212 | 0.062 | 0.030 | 0.050 | 2.025 | 0.980 | 1.633 | 0.031 | 0.84 | 970.1 |
| 2.5131 | 600 | 600 | 212 | 0 | 14.5 | 0.037 | 240 | 211 | 0.072 | 0.011 | 0.072 | 2.351 | 0.359 | 2.351 | 0.011 | 0.31 | 970.7 |
| 2.5132 | 617 | 595 | 211 | 1 | 14.6 | 0.037 | 219 | 212 | 0.071 | 0.023 | 0.074 | 2.319 | 0.751 | 2.417 | 0.023 | 0.65 | 970.5 |
| 2.5142 | 53 | 695 | 214 | 5 | 17.0 | 0.043 | 290 | 219 | 0.083 | 0.128 | 0.006 | 2.727 | 4.197 | 0.197 | 0.135 | 3.81 | 965.6 |
| 2.5143 | 56 | 650 | 215 | 3 | 16.7 | 0.042 | 300 | 218 | 0.078 | 0.117 | 0.007 | 2.555 | 3.832 | 0.229 | 0.124 | 3.48 | 966.2 |
| 2.5144 | 73 | 600 | 214 | 4 | 16.5 | 0.042 | 285 | 218 | 0.072 | 0.104 | 0.008 | 2.359 | 3.408 | 0.262 | 0.109 | 3.03 | 966.6 |
| 2.5145 | 83 | 595 | 214 | 4 | 16.3 | 0.041 | 285 | 217 | 0.071 | 0.093 | 0.010 | 2.325 | 3.046 | 0.328 | 0.098 | 2.68 | 967.0 |

TABLE B5

| Test | Qfd (gpm) | Qfin (gpm) | Tecc (F) | DTsub (F) | Plp (psia) | RHOg (#/FT3) | Tin (F) | Tsat (F) | J*fin | J*gc | J*fd | K*fin | K*gc | K*fd | J*gc (sup) | Wgc (#/sec) | Hfg (BTU/#) |
|---|---|---|---|---|---|---|---|---|---|---|---|---|---|---|---|---|---|
| 2.5062 | 53 | 1030 | 148 | 67 | 15.5 | 0.039 | 290 | 215 | 0.124 | 0.200 | 0.006 | 4.081 | 6.581 | 0.197 | 0.211 | 5.80 | 968.7 |
| 2.5063 | 182 | 1040 | 150 | 65 | 15.5 | 0.039 | 290 | 215 | 0.125 | 0.180 | 0.022 | 4.113 | 5.923 | 0.724 | 0.190 | 5.25 | 968.7 |
| 2.5064 | 440 | 1100 | 143 | 73 | 16.0 | 0.040 | 290 | 216 | 0.132 | 0.165 | 0.053 | 4.348 | 5.435 | 1.746 | 0.174 | 4.80 | 967.6 |
| 2.5065 | 615 | 1040 | 141 | 75 | 15.5 | 0.039 | 290 | 215 | 0.125 | 0.143 | 0.074 | 4.117 | 4.710 | 2.437 | 0.151 | 4.10 | 968.7 |
| 2.5066 | 510 | 1000 | 143 | 72 | 15.5 | 0.039 | 290 | 215 | 0.120 | 0.150 | 0.061 | 3.950 | 4.938 | 2.008 | 0.158 | 4.40 | 968.7 |
| 2.5067 | 70 | 1000 | 145 | 70 | 15.7 | 0.040 | 290 | 215 | 0.120 | 0.188 | 0.008 | 3.950 | 6.189 | 0.263 | 0.193 | 5.40 | 968.2 |
| 2.5068 | 1020 | 1000 | 150 | 62 | 14.5 | 0.037 | 290 | 211 | 0.120 | 0.000 | 0.123 | 3.941 | 0.000 | 4.039 | 0.000 | 0.00 | 970.7 |
| 2.5069 | 0 | 980 | 149 | 67 | 16.0 | 0.040 | 290 | 216 | 0.118 | 0.227 | 0.000 | 3.885 | 7.474 | 0.000 | 0.239 | 6.60 | 967.6 |
| 2.5070 | 31 | 1000 | 161 | 65 | 16.0 | 0.040 | 290 | 216 | 0.120 | 0.210 | 0.004 | 3.948 | 6.908 | 0.132 | 0.221 | 6.20 | 967.6 |
| 2.5082 | 124 | 950 | 145 | 70 | 15.5 | 0.039 | 290 | 215 | 0.114 | 0.205 | 0.015 | 3.753 | 6.749 | 0.494 | 0.216 | 5.90 | 968.7 |
| 2.5083 | 16 | 950 | 152 | 64 | 16.0 | 0.040 | 290 | 216 | 0.114 | 0.212 | 0.002 | 3.753 | 6.980 | 0.066 | 0.223 | 6.20 | 967.6 |
| 2.5084 | 676 | 986 | 143 | 73 | 16.0 | 0.040 | 290 | 216 | 0.116 | 0.145 | 0.081 | 3.887 | 4.776 | 2.668 | 0.153 | 4.44 | 967.6 |
| 2.5085 | 333 | 983 | 148 | 71 | 17.0 | 0.043 | 290 | 219 | 0.118 | 0.164 | 0.040 | 3.891 | 5.408 | 1.319 | 0.172 | 5.27 | 965.6 |
| 2.5086 | 182 | 989 | 145 | 73 | 16.5 | 0.042 | 290 | 218 | 0.118 | 0.168 | 0.022 | 3.891 | 5.539 | 0.725 | 0.177 | 5.43 | 966.6 |
| 2.5017 | 820 | 976 | 144 | 69 | 15.0 | 0.038 | 290 | 213 | 0.117 | 0.125 | 0.098 | 3.848 | 4.111 | 3.223 | 0.132 | 3.54 | 969.7 |
| 2.5018 | 958 | 963 | 142 | 71 | 15.0 | 0.038 | 290 | 213 | 0.116 | 0.000 | 0.115 | 3.815 | 0.000 | 3.782 | 0.000 | 0.00 | 969.7 |

TABLE B6

| Test | Qfd (gpm) | Qfin (gpm) | Tecc (F) | DTsub (F) | Plp (psia) | RHOg (#/FT3) | Tin (F) | Tsat (F) | J*fin | J*gc | J*fd | K*fin | K*gc | K*fd | J*gc (sup) | Wgc (#/sec) | Hfg (BTU/#) |
|---|---|---|---|---|---|---|---|---|---|---|---|---|---|---|---|---|---|
| 2.5133 | 700 | 1050 | 206 | 7 | 15.0 | 0.038 | 311 | 213 | 0.126 | 0.033 | 0.084 | 4.122 | 1.079 | 2.748 | 0.035 | 0.92 | 969.7 |
| 2.5134 | 1042 | 1085 | 208 | 7 | 14.5 | 0.037 | 308 | 211 | 0.130 | 0.022 | 0.125 | 4.248 | 0.719 | 4.085 | 0.024 | 0.60 | 970.7 |
| 2.5135 | 1017 | 1090 | 204 | 8 | 14.7 | 0.037 | 292 | 212 | 0.131 | 0.028 | 0.122 | 4.283 | 0.915 | 3.989 | 0.030 | 0.78 | 970.3 |
| 2.5136 | 717 | 1080 | 206 | 7 | 15.0 | 0.038 | 313 | 213 | 0.130 | 0.031 | 0.086 | 4.252 | 1.014 | 2.813 | 0.033 | 0.87 | 969.7 |
| 2.5137 | 225 | 1020 | 207 | 6 | 15.4 | 0.039 | 300 | 214 | 0.122 | 0.043 | 0.027 | 3.991 | 1.407 | 0.883 | 0.046 | 1.21 | 968.9 |
| 2.5138 | 192 | 1050 | 207 | 8 | 15.5 | 0.039 | 297 | 215 | 0.126 | 0.048 | 0.023 | 4.124 | 1.571 | 0.753 | 0.051 | 1.38 | 968.7 |
| 2.5139 | 283 | 1075 | 206 | 8 | 15.3 | 0.039 | 287 | 214 | 0.129 | 0.041 | 0.034 | 4.222 | 1.342 | 1.113 | 0.043 | 1.15 | 969.1 |
| 2.5140 | 550 | 1070 | 206 | 7 | 15.2 | 0.039 | 313 | 213 | 0.128 | 0.039 | 0.066 | 4.187 | 1.276 | 2.159 | 0.042 | 1.11 | 969.3 |
| 2.5141 | 167 | 1040 | 204 | 11 | 15.6 | 0.039 | 287 | 215 | 0.125 | 0.049 | 0.020 | 4.093 | 1.604 | 0.655 | 0.052 | 1.39 | 968.8 |
| 2.5001 | 94 | 950 | 205 | 14 | 17.0 | 0.043 | 290 | 219 | 0.113 | 0.101 | 0.011 | 3.708 | 3.314 | 0.361 | 0.106 | 3.10 | 965.6 |
| 2.5002 | 294 | 1000 | 204 | 11 | 15.5 | 0.039 | 290 | 215 | 0.119 | 0.052 | 0.035 | 3.897 | 1.703 | 1.146 | 0.055 | 1.62 | 968.7 |
| 2.5003 | 5 | 990 | 205 | 17 | 18.0 | 0.045 | 290 | 222 | 0.118 | 0.144 | 0.001 | 3.878 | 4.732 | 0.033 | 0.151 | 4.70 | 963.7 |
| 2.5004 | 61 | 960 | 206 | 15 | 17.5 | 0.044 | 290 | 221 | 0.114 | 0.107 | 0.007 | 3.745 | 3.515 | 0.230 | 0.112 | 3.48 | 964.7 |
| 2.5005 | 148 | 925 | 207 | 12 | 17.0 | 0.043 | 290 | 219 | 0.110 | 0.074 | 0.018 | 3.608 | 2.427 | 0.590 | 0.078 | 2.40 | 965.6 |
| 2.5006 | 0 | 850 | 209 | 13 | 18.0 | 0.045 | 290 | 222 | 0.101 | 0.133 | 0.000 | 3.318 | 4.369 | 0.000 | 0.139 | 4.40 | 963.7 |
| 2.5007 | 184 | 950 | 205 | 13 | 16.5 | 0.042 | 290 | 218 | 0.113 | 0.070 | 0.022 | 3.706 | 2.296 | 0.722 | 0.074 | 2.22 | 966.6 |
| 2.5008 | 608 | 1009 | 205 | 11 | 16.0 | 0.040 | 290 | 216 | 0.120 | 0.039 | 0.075 | 3.931 | 1.278 | 2.457 | 0.041 | 1.23 | 967.6 |
| 2.5009 | 0 | 1020 | 205 | 17 | 18.0 | 0.045 | 290 | 222 | 0.121 | 0.160 | 0.000 | 3.977 | 5.258 | 0.000 | 0.168 | 5.22 | 963.7 |
| 2.5010 | 885 | 1000 | 202 | 10 | 14.5 | 0.037 | 290 | 211 | 0.120 | 0.027 | 0.106 | 3.923 | 0.883 | 3.465 | 0.029 | 0.85 | 970.7 |
| 2.5011 | 908 | 1010 | 204 | 8 | 14.5 | 0.037 | 290 | 211 | 0.120 | 0.024 | 0.109 | 3.921 | 0.784 | 3.562 | 0.025 | 0.67 | 970.7 |
| 2.5012 | 908 | 1010 | 203 | 9 | 14.5 | 0.037 | 290 | 211 | 0.120 | 0.000 | 0.109 | 3.921 | 0.000 | 3.562 | 0.000 | 0.00 | 970.7 |
| 2.5013 | 0 | 1007 | 202 | 20 | 18.0 | 0.045 | 290 | 222 | 0.120 | 0.163 | 0.000 | 3.945 | 5.359 | 0.000 | 0.171 | 5.38 | 963.7 |

# APPENDIX C

## STATISTICAL ANALYSIS OF 1/5 SCALE DATA

The statistical analysis of 1/30, 1/15, and 2/15 scale ECC bypass data has been previously documented (Reference 8). That analysis indicated that J* scaling of the hydraulics may begin breaking down at 1/15 scale. Beyond that scale, $J^*\sqrt{S}$ scaling (constant momentum flux) may be more appropriate.* The effect of condensation was observed to increase with increasing scale size. These findings support NRC's current licensing practice of assuming constant momentum flux to extrapolate ECC bypass hydraulics to full scale. Countercurrent flow tests performed in Creare's 1/5-scale facility have provided additional confidence in these findings. The statistical analysis of the 1/5-scale data and a comparison of the results which have been obtained for the different scale facilities are presented in this Appendix.

The same statistical techniques used in Reference 8 have also been used to analyze the 1/5-scale ECC bypass data. To be consistent with the previous study two correlations were used to model the 1/5-scale data. The first is a traditional formulation with improved slope dependency and a constant condensation efficiency. It is described as follows:

$$[J_g^* - F\, J_{g,T}^*(\mathrm{COND})]^{\frac{1}{2}} + [M - Z\, J_{g,T}^*(\mathrm{COND})\, \exp(-a\sqrt{(J_\ell^*)_{in}})]J_\ell^{*\frac{1}{2}} = C \qquad \text{(C-1)}$$

Modifications based on observations of data trends (particularly air-water data) have been applied to this equation. This yields the second correlation:

$$J_g^{*\frac{1}{2}} - FJ_{g,T}^*(\mathrm{COND})^{\frac{1}{2}} + [M - Z\, J_{g,T}^*(\mathrm{COND})\, \exp(-a\sqrt{(J_\ell^*)_{in}})]J_\ell^{*\frac{1}{2}} = C \qquad \text{(C-2)}$$

Although the air-water data has not been included, the same correlational form has been maintained since it models the data quite well.**

These correlations were used in a non-linear numerical regression routine (Reference 8) to determine the empirical constants "F", "M", "Z", "C", and "a". Tables C-1 and C-2 present a comparison of the values calculated using the 1/5-scale data and those calculated using smaller scale data. Statistics which indicate how well the models described the data are presented in Appendix D. A listing of the Creare 1/5-scale data was provided in Appendix B.

The calculated empirical constants were plotted as functions of scale size in Figures C-1 to C-8. The scale size is determined by dividing the average annulus circumference in the experiment by that in a reactor (about 43 ft).

---

*We used $J^*\sqrt{S}$ rather than K* since we have no basis to prove or disprove the validity of the small surface tension effect in K*. For all practical purposes, $J^*\sqrt{S}$ scaling is equivalent to K* scaling and is also dimensionless.

**The previous BCL 1/15 and 2/15 air-water data has not been included in the overall evaluation of the data base here for two reasons. First, the density of the air is influenced by humidity. This may affect the validity of the results. Second, a sufficient amount of steam-water data at nearly saturated conditions is available. This reduces the need for using air-water data.

TABLE C-1

EMPIRICAL CONSTANTS CALCULATED FOR THE TRADITIONAL ECC BYPASS FORMULATION OF EQUATION (C-1)*

| Coefficient | Creare 1/5 Steam | BCL 2/15 Steam | BCL 1/15 Steam | Creare 1/15 Steam | Creare 1/30 Steam |
|---|---|---|---|---|---|
| C | .368±.009 | .455±.010 | .523±.012 | .434±.017 | .388±.014 |
| F | .238±.048 | .297±.014 | .119±.013 | .146±.019 | .064±0.64 |
| M | .894±.082 | .987±.078 | 1.18±.086 | 1.009±.094 | .395±.091 |
| Z | 1.37 ±.515 | 11.73±2.90 | 19.13±2.04 | 11.22±2.48 | 2.58±1.40 |
| a | 0.0 | 9.5 | 8.0 | 6.0 | 3.0 |

*95% Confidence Limits (±two standard errors).

TABLE C-2

EMPIRICAL CONSTANTS CALCULATED FOR THE MODIFIED ECC BYPASS FORMULATION OF EQUATION (C-2)*

| Coefficient | Creare 1/5 Steam | BCL 2/15 Steam | BCL 1/15 Steam | Creare 1/15 Steam | Creare 1/30 Steam |
|---|---|---|---|---|---|
| C | .344±.014 | .328±.012 | .417±.013 | .401±.017 | .390±.016 |
| F | .209±.047 | .382±.022 | .233±.019 | .155±.027 | .036±.048 |
| M | .822±.092 | .666±.053 | .877±.059 | .816±.091 | .417±.090 |
| Z | 1.49±0.42 | 4.05±1.29 | 16.91±2.22 | 5.33±0.91 | 3.35±1.13 |
| a | 0.0 | 7.5 | 9.0 | 4.5 | 3.0 |

*95% Confidence Limits (±two standard errors).

The 100% bypass point without condensation ($C^2$), has been plotted as a function of scale size in Figures C-1 and C-2. The traditional formulation of Figure C-1 indicates that the value of "C" is different for the BCL and Creare data sets. The modified formulation of Figure C-2 suggests that "C" is the same for the BCL and Creare data sets. Both figures support the conclusion that as scale increases, there is a transition from J* scaling to $J^*\sqrt{S}$ scaling. The transition occurs at a scale size of about 1/15.

The condensation efficiency has also been plotted as a function of scale size. We observe in Figures C-3 and C-4 that condensation effects increase with increasing scale size for both the BCL and Creare facilities. The increase has about the same magnitude for the traditional formulation in Figure C-3. The increase is somewhat larger for BCL data than Creare data by the modified formulation of Figure C-4.

The slope of the penetration curve without condensation, M, as a function of scale size is presented in Figures C-5 and C-6. BCL and Creare data are in good agreement by either correlation form. These figures suggest an apparent scale dependency. One possible explanation for this trend can be found by examining a model developed by BCL (Reference 9). This model utilizes a slope which is not constant but a weak function of liquid flow down ($K^*_{ld}$ for K* scaling used by BCL) as shown in Figure C-7. This model is supported by observation of distorted geometry data. The constant slope of near unity used in the analysis herein, while a good assumption, is an approximation. Also shown in Figure C-7 is the range of liquid flow down for the bulk of the tests at various scales. As shown in the figure, the maximum liquid flow down increases with scale size due to the fact that J* scaling was used to set test conditions. Thus, this model would suggest that the average value of M would decrease as scale increases as observed in Figures 5 and 6. The model also indicates a reverse of this trend (M increases as scale increases) for very small sizes as supported by the 1/30-scale data in Figures C-5 and C-6. The apparent scale dependency of M is thus hypothesized to be an injection flow effect arising due to the use of J* scaling to set the experimental conditions.

Figures C-8 and C-9 show the effect of condensation on the slope (Z and a). These plots show trends opposite that of the F term. This was expected since an increasing F term indicates that the process is approaching equilibrium at the 100% bypass point. As equilibrium is approached, the effect of condensation on slope will decrease.

Although some differences in the results from BCL and Creare facilities exist, correlations of data from both point to the same scaling trends for the individual empirical constants. A brief description of the possible facility differences is presented here for completeness.

Since the BCL and Creare data for similar scales (1/15) result in different correlation constants, differences in the facilities or test procedures must exist. Several possible causes for the dissimilar correlation constants have been examined. The first is variations in cold leg geometries. The BCL facilities have a 60°-120° cold leg arrangement whereas the Creare facilities have a 90°-90° cold leg arrangement. Two comparisons have been made to determine if dissimilar cold leg geometries can significantly influence the test results. Figure C-10 compares the BCL 1/15-scale correlation (whose constants were derived using BCL steady state and filling data from a 60°-120° cold

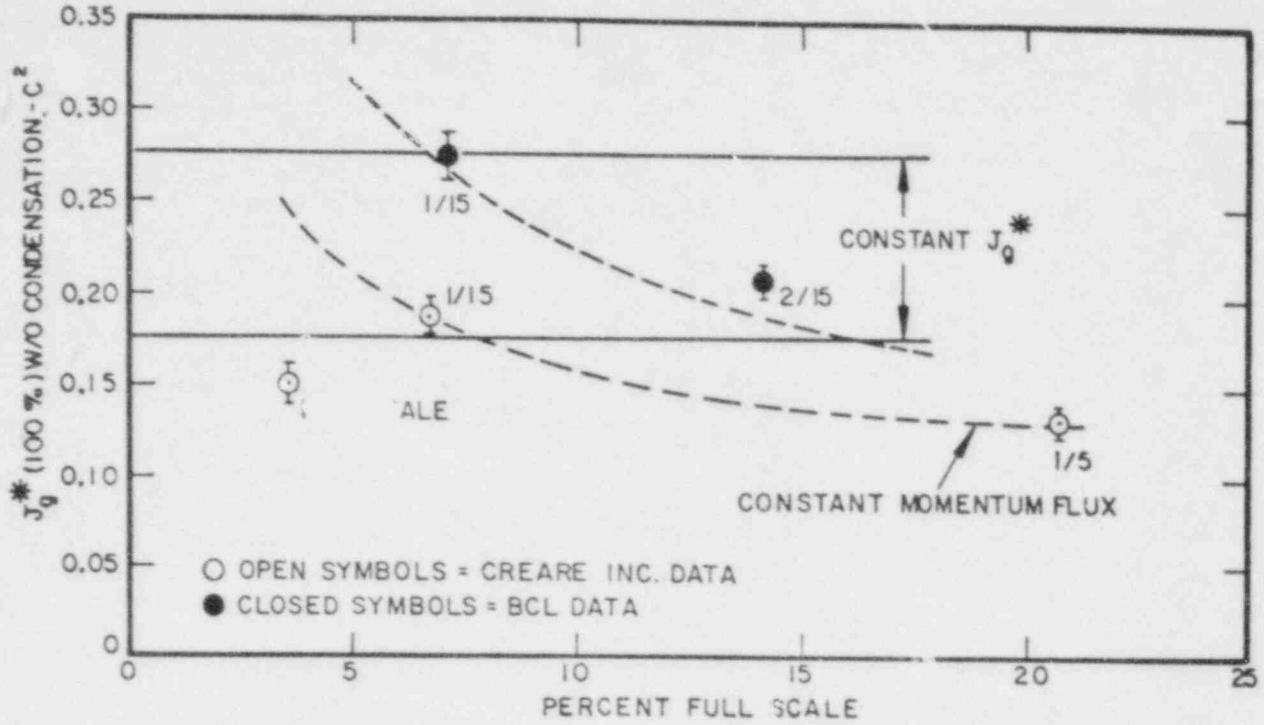


Figure C-1. GAS FLOW FOR COMPLETE BYPASS (WITHOUT CONDENSATION) AS A FUNCTION OF SCALE SIZE USING EQUATION C-1

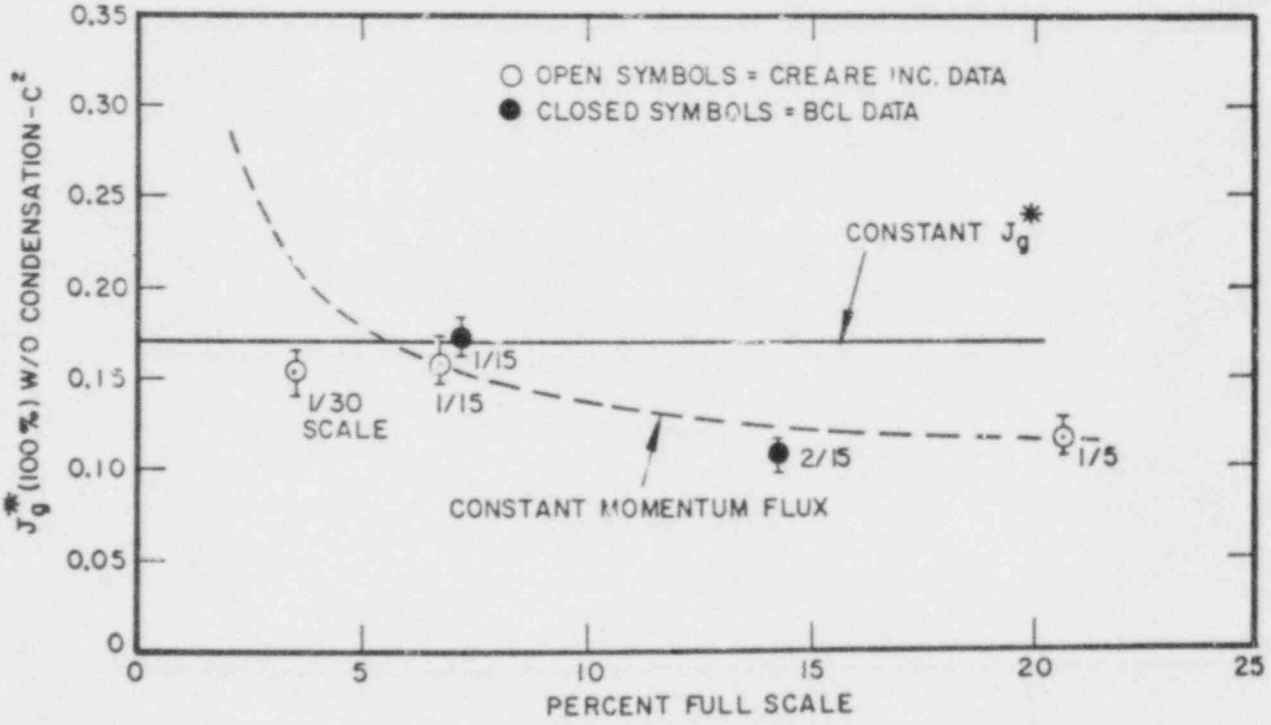


Figure C-2. GAS FLOW FOR COMPLETE BYPASS (WITHOUT CONDENSATION) AS A FUNCTION OF SCALE SIZE USING EQUATION C-2

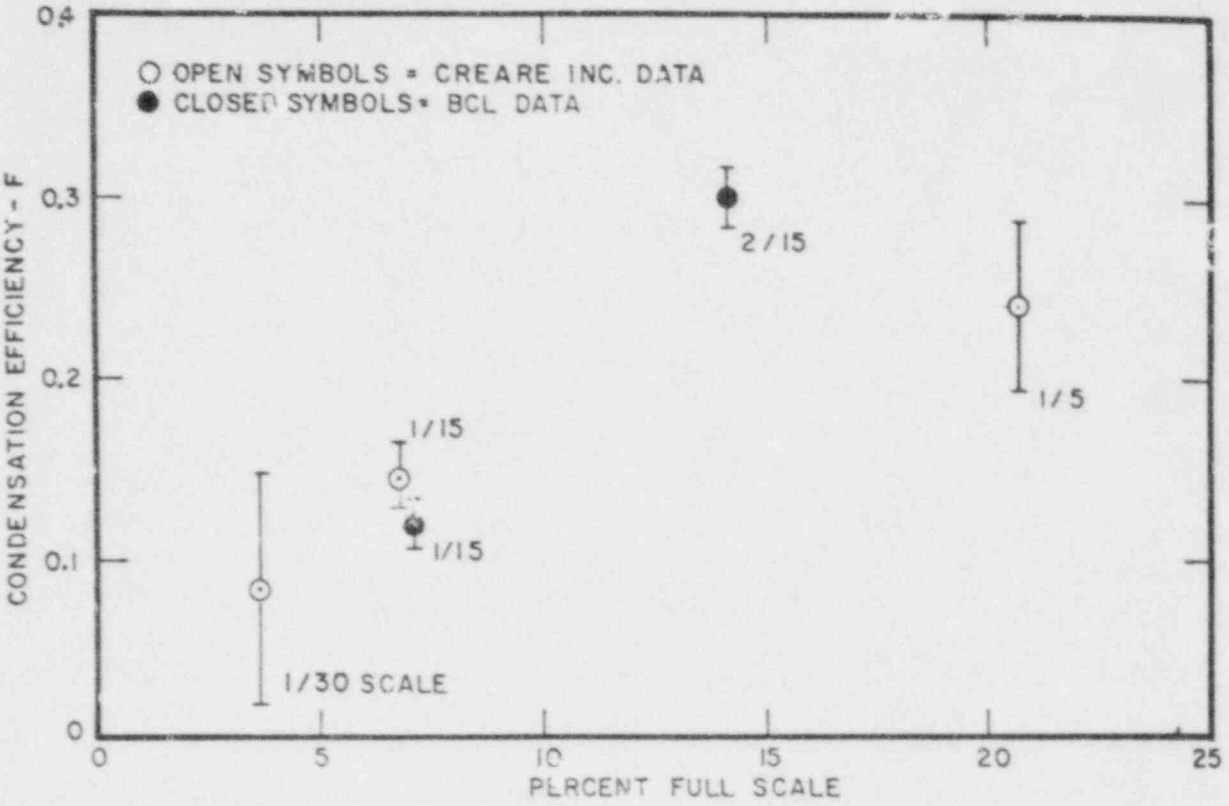


Figure C-3. CONDENSATION EFFICIENCY AS A FUNCTION OF SCALE SIZE USING EQUATION C-1

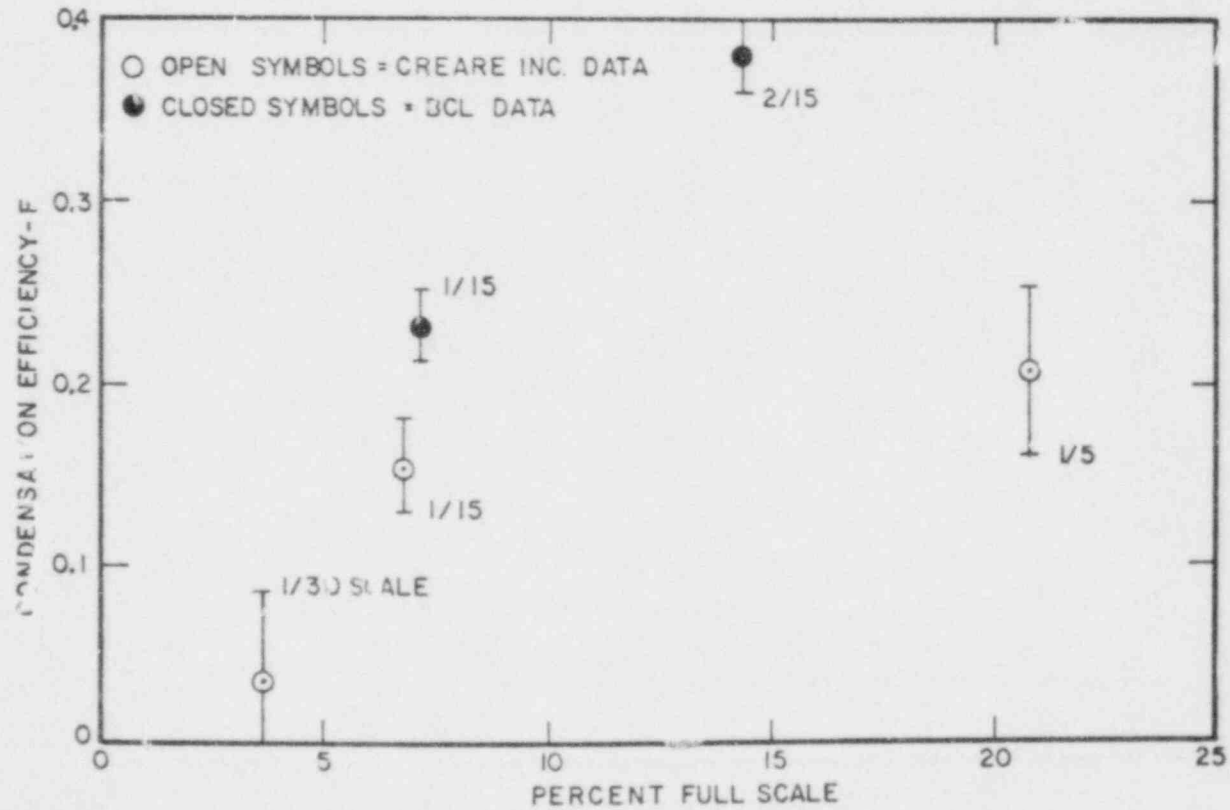


Figure C-4. CONDENSATION EFFICIENCY AS A FUNCTION OF SCALE SIZE USING EQUATION C-2

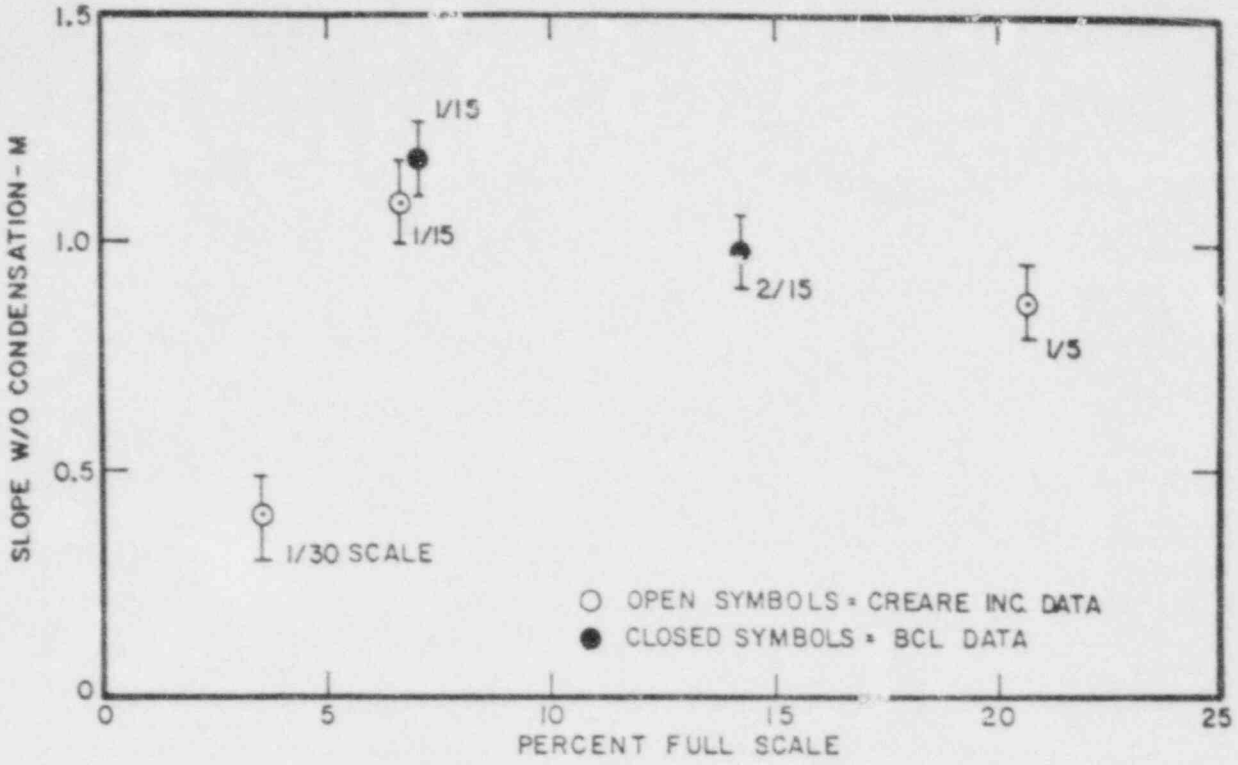


Figure C-5. SLOPE OF PENETRATION CURVE (WITHOUT CONDENSATION) AS A FUNCTION OF SCALE SIZE USING EQUATION C-1

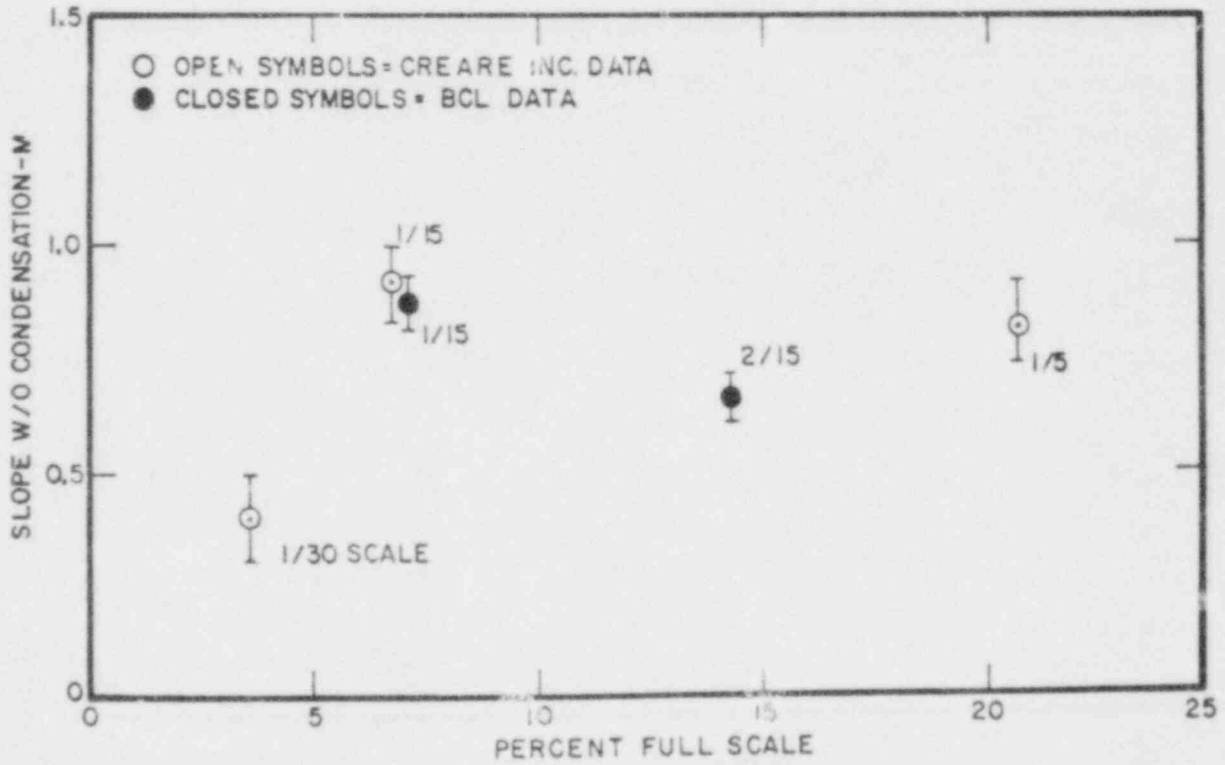


Figure C-6. SLOPE OF PENETRATION CURVE (WITHOUT CONDENSATION) AS A FUNCTION OF SCALE SIZE USING EQUATION C-2

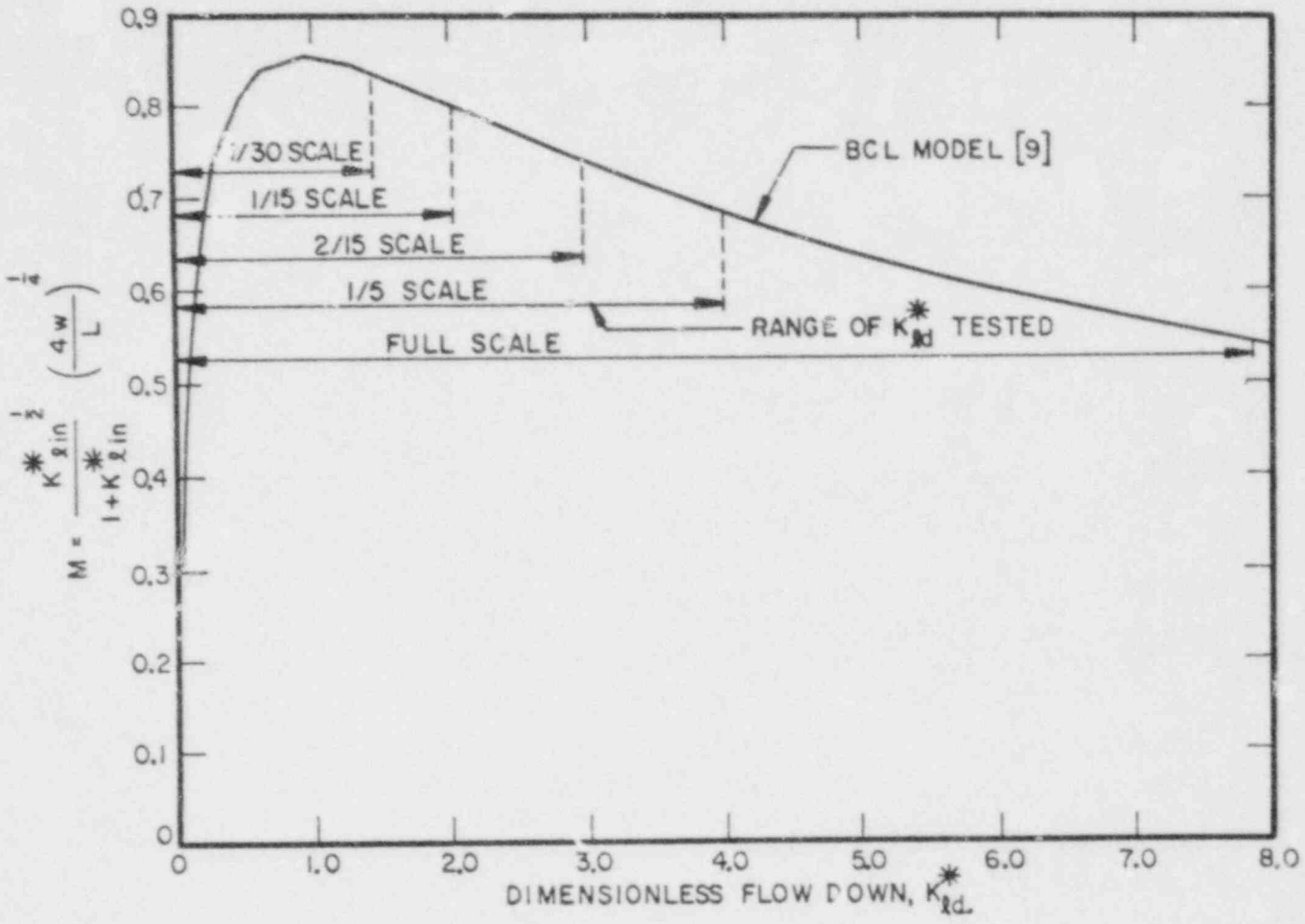


Figure C-7. CALCULATED SLOPE OF PENETRATION CURVE AS A FUNCTION OF ECC PENETRATION FLOW AT VARIOUS SCALES USING BCL MODEL [9]

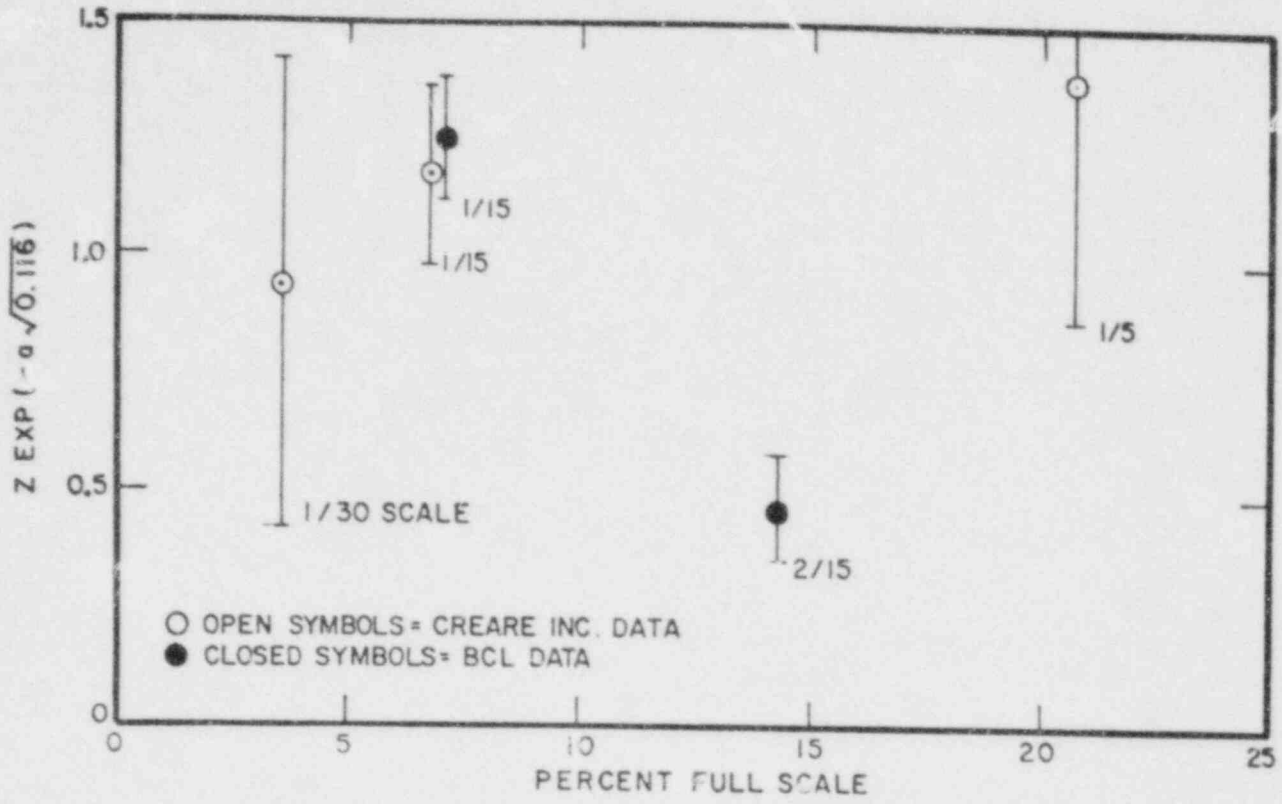


Figure C-8. EFFECT OF CONDENSATION ON SLOPE OF PENETRATION CURVE AS A FUNCTION OF SCALE SIZE USING EQUATION C-1

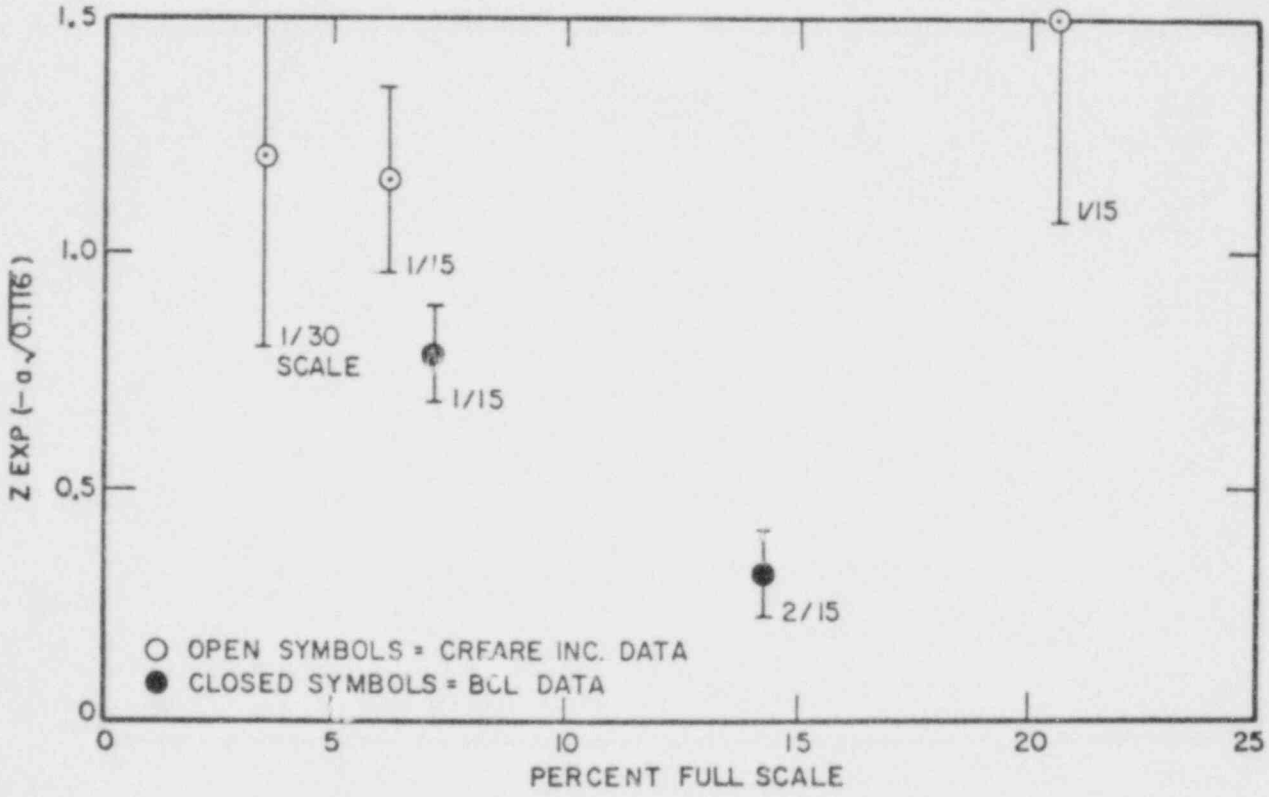


Figure C-9. EFFECT OF CONDENSATION ON SLOPE OF PENETRATION CURVE AS A FUNCTION OF SCALE SIZE USING EQUATION C-2

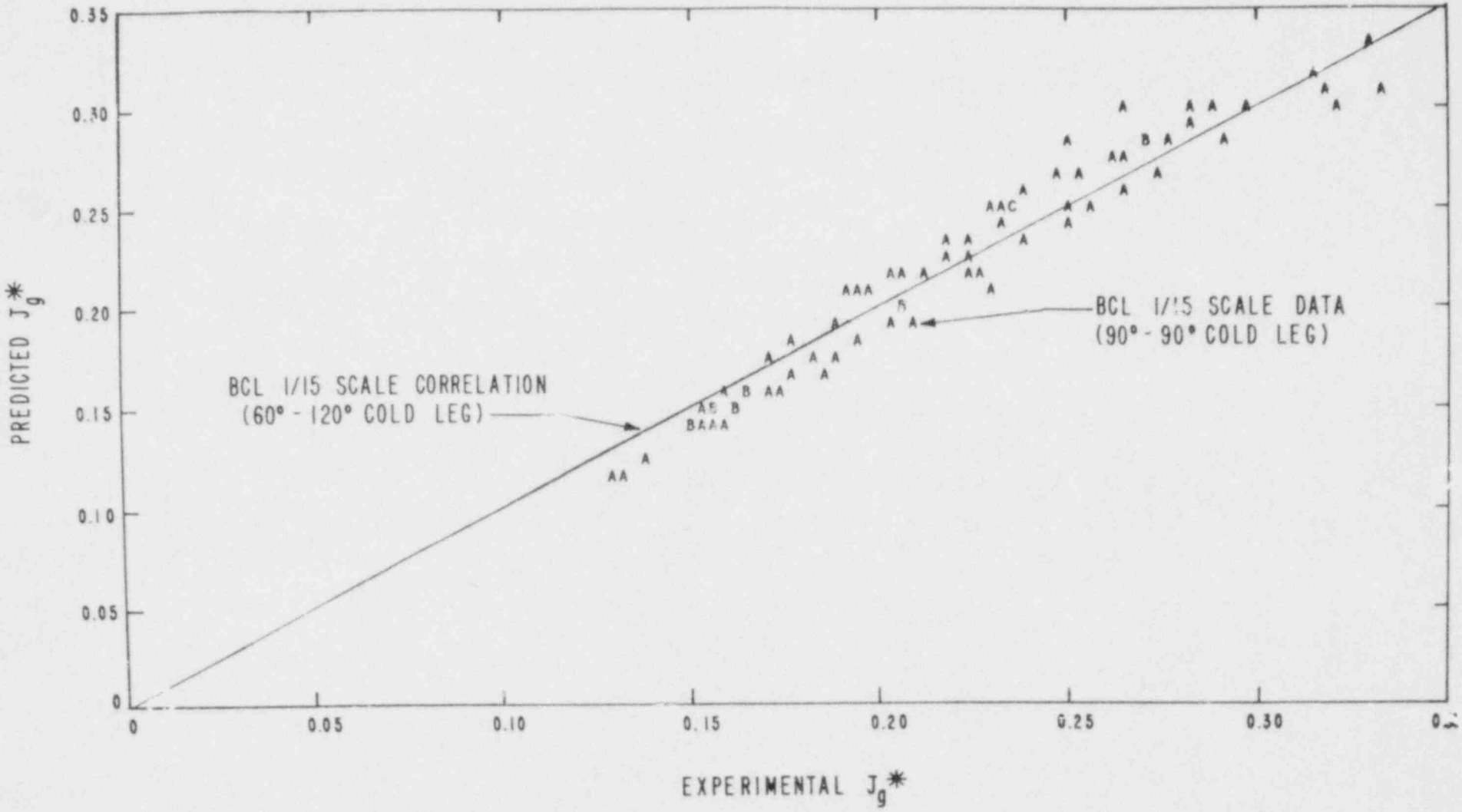


Figure C-10 - COMPARISON OF BCL 1/15 (60°-120° COLD LEG) CORRELATION WITH BCL 1/15 (90°-90° COLD LEG) DATA

leg geometry) with data obtained in the BCL 90-90° cold leg facility. This figure shows that the constants obtained from the 60-120° cold leg data reasonably describe data from the 90-90° cold leg facility. Therefore, the cold leg geometry does not influence the test results. Figure C-11 compares the Creare 1/15-scale correlation (whose constants were derived using Creare data from a 90-90° cold leg geometry) with data otherwise in the BCL 90-90° cold leg facility. Although the Creare correlation and the BCL data are both from 90-90° cold leg facilities, Figure C-10 shows that differences in the results from these facilities still exist.

Minor differences in the scaling of the BCL and Creare facilities might have a possible influence on the test results. For example, the downcomer gap and the annular circumference of the BCL 1/15-scale model are slightly larger than those of the Creare 1/15-scale model. Current scaling theories, however, indicate that small dimensional differences would have very little or no influence on the test results since dimensions appear to the one-quarter power. The results of wide variations in tested scale size and changes in length and gap by factors of two also indicate that these minor dimensional differences should not influence the results.

Since dimensional aspects do not appear to be the cause of the difference in the BCL and Creare data, the test procedures used by each facility have been reviewed. BCL tests are performed in either a filling mode or a steady-state mode. Creare operates only in the filling mode. During the filling mode of operation, a constant flow rate of steam is forced through the vessel. Simultaneously, water is injected into three cold legs at a constant preset flow. The test is run until the plenum fills. During BCL steady-state operations, steam and water are injected into the vessel as in the filling mode. However, the water level in the lower plenum is maintained at a constant level by draining. The test is run until an equilibrium filling rate is obtained.

We have examined the BCL filling and steady state data in detail to determine if the mode of operation influenced the data. BCL filling data does appear to differ slightly from the BCL steady state data and is in the direction of the Creare filling data. However, the magnitude of the difference between BCL filling and steady state data is smaller than the difference between BCL and Creare data. This analysis is hampered by a less complete BCL filling data base and due to the fact that the differences we are examining are on the same order as the scatter inherent in both data sets.

We have not been able to conclusively determine the cause of what appears to be a basic difference between the BCL and Creare data, although the mode of operation is still considered to be a likely cause. While this is disconcerting, it does not affect the conclusions we draw from the data. Viewed as two separate data bases, BCL and Creare data support similar trends with scale. Viewed as a single data set, we also see similar scale behavior with simply a larger data scatter.

## Conclusion

Statistical analyses of the new countercurrent flow data in the largest facility tested to date (1/5 scale) support the trends previously identified in statistical analyses of data in facilities from 1/30 to 2/15-scale [8]. One significant trend is that a transition to constant momentum flux scaling at about 1/15 scale continues up to 1/5 scale. This supports the conservative use by NRC of a constant momentum flux to scale

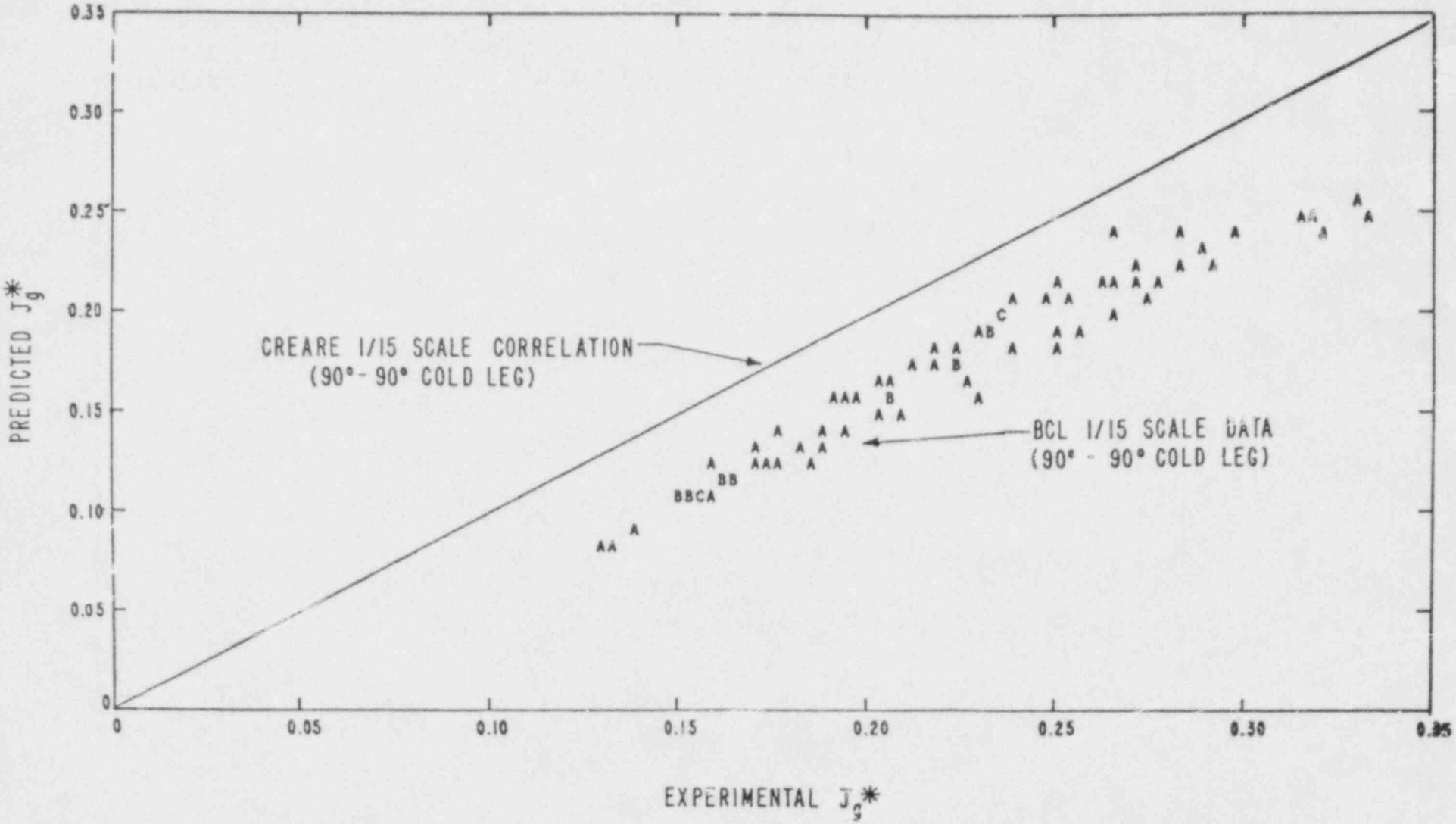


Figure C-11. COMPARISON OF CREARE 1/15 (90°-90° COLD LEG) CORRELATION WITH BCL 1/15 (90°-90° COLD LEG) DATA

the hydraulics of ECC bypass to full scale in licensing calculations. The other significant trend is that the effect of condensation increases somewhat with scale. This acts to partially offset the first trend in the experimental data. The end of bypass occurs at a larger steam flux with condensation than without. Table C-3 contains recommendations for extrapolating the correlational constants in Tables C-1 and C-2 to full scale based on observed scaling trends.

TABLE C-3

RECOMMENDED METHODS TO EXTRAPOLATE CORRELATIONAL COEFFICIENTS IN TABLES C-1 AND C-2 TO LARGER SCALE

| Coefficient | Value at Large Scale | Scaling Basis |
|---|---|---|
| C | Use values from Creare 1/5 or BCL 2/15 data (whichever is smaller for conservatism) modified to decrease by the fourth root of scale size (circumference) | Observed scaling behavior (also more of scaling theories) |
| F | Use values from Creare 1/5 or BCL 2/15 (smaller 1/5 values for more conservatism) | Observed increase in F with scale size. Thus values no larger than at small scale should be conservative. |
| M | Use values from Creare 1/5 or BCL 2/15 (larger value is more conservative) | Constant or slightly decreasing value observed |
| Z | ZERO | Observed decrease with scale size (also more conservative) |
| a | Not used when Z=0.0 | |

Caution--values of coefficients derived for one equation should not be used in the other equation. We currently have no basis to support one equation over another.

# APPENDIX D

## CREARE 1/5 SCALE NON-LINEAR LEAST SQUARES STATISTICS

CREARE 1/5 SCALE DATA: NLIN 11:43 TUESDAY, MAY 26, 1981

USING THE TRADITIONAL FORMULATION OF NLIN AND A=0.0

NON-LINEAR LEAST SQUARES SUMMARY STATISTICS DEPENDENT VARIABLE JG

| SOURCE | DF | SUM OF SQUARES | MEAN SQUARE |
|---|---|---|---|
| REGRESSION | 4 | 1.09496238 | 0.27374060 |
| RESIDUAL | 103 | 0.02090162 | 0.00020293 |
| UNCORRECTED TOTAL | 107 | 1.11586400 | |
| (CORRECTED TOTAL) | 106 | 0.30511077 | |

| PARAMETER | ESTIMATE | ASYMPTOTIC STD. ERROR | ASYMPTOTIC 95 % CONFIDENCE INTERVAL LOWER | UPPER |
|---|---|---|---|---|
| F | 0.23775776 | 0.02401899 | 0.19012146 | 0.28539406 |
| C | 0.36773046 | 0.00476312 | 0.35828388 | 0.37717704 |
| Z | 1.37067312 | 0.25770109 | 0.85958056 | 1.88176568 |
| M | 0.89404533 | 0.04186451 | 0.81101643 | 0.97707424 |

ASYMPTOTIC CORRELATION MATRIX OF THE PARAMETERS

| | F | C | Z | M |
|---|---|---|---|---|
| F | 1.000000 | -0.517138 | -0.836945 | -0.329976 |
| C | -0.517138 | 1.000000 | 0.513061 | 0.758957 |
| Z | -0.836945 | 0.513061 | 1.000000 | 0.556185 |
| M | -0.329976 | 0.758957 | 0.556185 | 1.000000 |

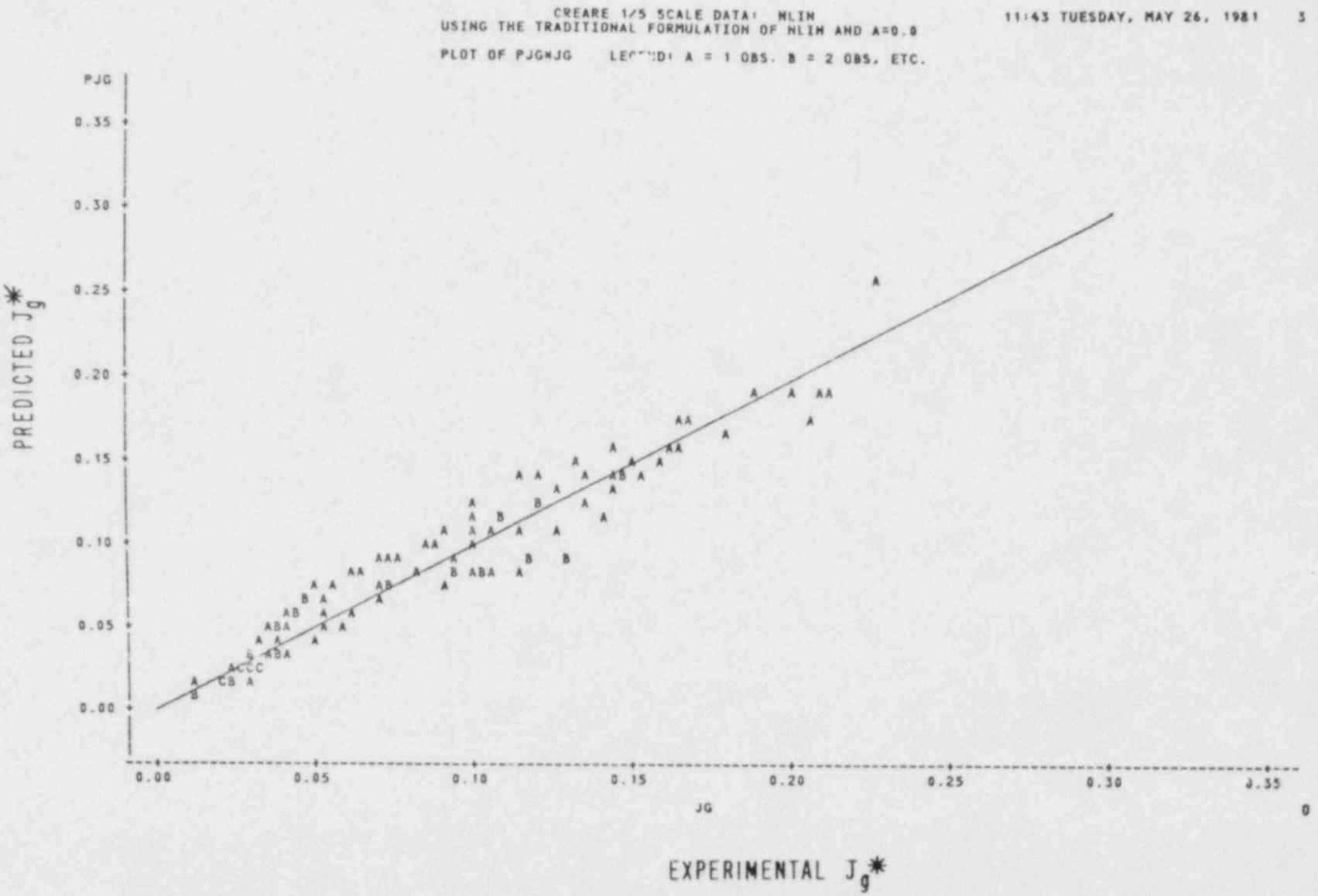


Figure D-1. COMPARISON OF CREARE 1/5 SCALE DATA WITH THE TRADITIONAL FORMULATION OF EQUATION C-1

CREARE 1/5 SCALE DATA 10:30 WEDNESDAY, JANUARY 14, 1981
USING THE MODIFIED FORMULATION OF NLIN3 AND A=0.0

NON-LINEAR LEAST SQUARES SUMMARY STATISTICS DEPENDENT VARIABLE JG

| SOURCE | DF | SUM OF SQUARES | MEAN SQUARE |
|---|---|---|---|
| REGRESSION | 4 | 1.09012077 | 0.27253019 |
| RESIDUAL | 103 | 0.02574323 | 0.00024993 |
| UNCORRECTED TOTAL | 107 | 1.11586400 | |
| (CORRECTED TOTAL) | 106 | 0.30511077 | |

| PARAMETER | ESTIMATE | ASYMPTOTIC STD. ERROR | ASYMPTOTIC 95 % CONFIDENCE INTERVAL LOWER | UPPER |
|---|---|---|---|---|
| F | 0.20874357 | 0.02353619 | 0.16206478 | 0.25542235 |
| C | 0.34370825 | 0.00719478 | 0.32943902 | 0.35797751 |
| Z | 1.49446501 | 0.21401141 | 1.07002119 | 1.91890886 |
| M | 0.83326462 | 0.04616018 | 0.74171621 | 0.92481304 |

ASYMPTOTIC CORRELATION MATRIX OF THE PARAMETERS

| | F | C | Z | M |
|---|---|---|---|---|
| F | 1.000000 | -0.816455 | -0.821209 | -0.500845 |
| C | -0.816455 | 1.000000 | 0.736986 | 0.762843 |
| Z | -0.821209 | 0.736986 | 1.000000 | 0.727995 |
| M | -0.500845 | 0.762843 | 0.727995 | 1.000000 |

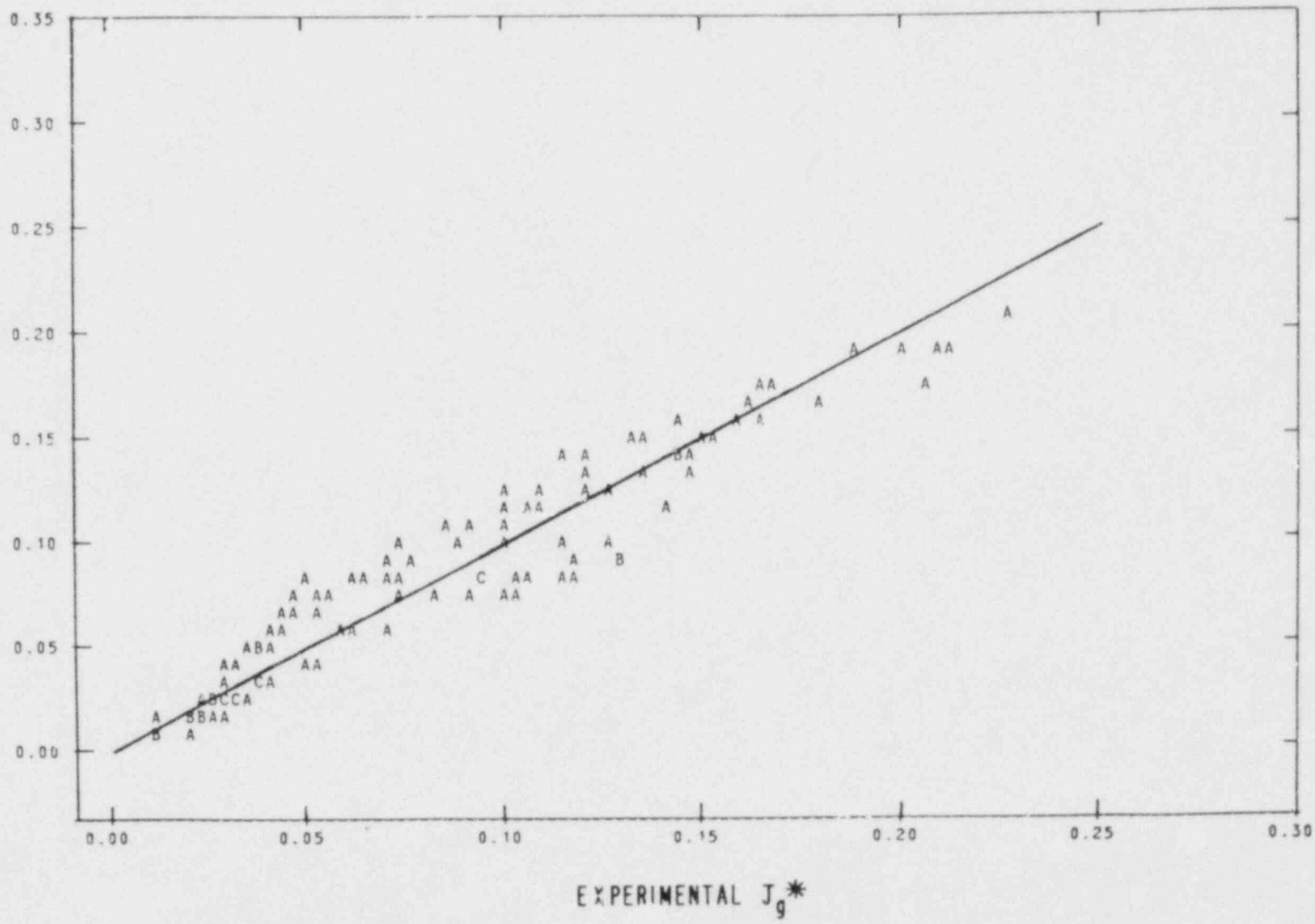


Figure D-2. COMPARISON OF CREARE 1/5 SCALE DATA WITH THE MODIFIED FORMULATION OF EQUATION C-2

NRC FORM 335 (7.77) U.S. NUCLEAR REGULATORY COMMISSION

**BIBLIOGRAPHIC DATA SHEET**

1. REPORT NUMBER (Assigned by DDC)
NUREG/CR-2106
Creare TN-333

4. TITLE AND SUBTITLE (Add Volume No., if appropriate)
1/5-Scale Countercurrent Flow Data Presentation and Discussion

2. (Leave blank)

3. RECIPIENT'S ACCESSION NO.

7. AUTHOR(S)
C.J. Crowley, P.H. Rothe, R.G. Sam

5. DATE REPORT COMPLETED
MONTH: April | YEAR: 1981

9. PERFORMING ORGANIZATION NAME AND MAILING ADDRESS (Include Zip Code)
Creare, Inc.
P.O. Box 71
Hanover, NH 03755

DATE REPORT ISSUED
MONTH: November | YEAR: 1981

6. (Leave blank)

8. (Leave blank)

12. SPONSORING ORGANIZATION NAME AND MAILING ADDRESS (Include Zip Code)
Office of Nuclear Regulatory Research
Division of Accident Evaluation
U.S. Nuclear Regulatory Commission
Washington, DC 20555

10. PROJECT/TASK/WORK UNIT NO.

11. CONTRACT NO.
FIN A4070

13. TYPE OF REPORT
Topical Report

PERIOD COVERED (Inclusive dates)

15. SUPPLEMENTARY NOTES

14. (Leave blank)

16. ABSTRACT (200 words or less)

Separate effects data for countercurrent flow behavior in a 1/5-scale PWR geometry are presented. The data represent the largest scale data of this type obtained up to the present time. A statistical analysis of these data has been performed and is also included here. The results of the statistical analysis are compared with analyses of data from smaller scale vessels. The trends in the data are consistent with trends indicated by the smaller scale data.

17. KEY WORDS AND DOCUMENT ANALYSIS

17a. DESCRIPTORS

17b. IDENTIFIERS/OPEN-ENDED TERMS

18. AVAILABILITY STATEMENT
Unlimited

19. SECURITY CLASS (This report)
Unclassified

21. NO. OF PAGES

20. SECURITY CLASS (This page)
Unclassified

22. PRICE
$